SIAM J. SCI. COMPUT.
Vol. 43, No. 1, pp. B167–B193

DECOUPLED, LINEAR, AND UNCONDITIONALLY ENERGY STABLE FULLY DISCRETE FINITE ELEMENT NUMERICAL SCHEME FOR A TWO-PHASE FERROHYDRODYNAMICS MODEL*

GUO-DONG ZHANG†, XIAOMING HE‡, AND XIAOFENG YANG§

Abstract. We consider in this paper numerical approximations of a phase field model for two-phase ferrofluids, which consists of the Navier–Stokes equations, the Cahn–Hilliard equation, the magnetostatic equations, and the magnetic field equation. By combining the projection method for the Navier–Stokes equations and some subtle implicit-explicit treatments for coupled nonlinear terms, we construct a linear, decoupled, fully discrete finite element scheme to solve the highly nonlinear and coupled multiphysics system efficiently. The scheme is provably unconditionally energy stable and leads to a series of decoupled linear equations to solve at each time step. Through numerous numerical examples in simulating benchmark problems such as the Rosensweig instability and droplet deformation, we demonstrate the stability and accuracy of the numerical scheme.

Key words. ferrofluid, phase field, unconditional energy stability, magnetic field, ferrohydrodynamics

AMS subject classifications. 65N12, 65M12, 65M70

DOI. 10.1137/19M1288280

1. Introduction.

Ferrofluids (also called magnetic fluids) are colloidal solutions made of ferromagnetic nanoparticles suspended in a dispersing liquid (usually an organic solvent or water). Such fluids can be controlled directly by the application of a magnetic field. Their basic properties, including the high magnetic polarization of saturation and zero remanences, predestine their applications in some systems that need precise control, such as optics, drug delivery, and electronic devices [35, 38, 41]. Some emerging applications of ferrofluids can be found in nanotechnologies and biomedical engineering, including assembly of micro/nanoparticles [8, 9, 31, 65], fluid transport and control [26, 27, 30, 36], and the treatment of retinal detachment [32], etc.

The hydrodynamics of magnetic suspension, known as ferrohydrodynamics (FHD), was well established by two generally accepted constitutive models, the Rosensweig [4, 5, 10, 40, 41, 42, 54] and Shliomis [3, 52, 53] models, which both treat ferrofluids as

*Submitted to the journal's Computational Methods in Science and Engineering section September 23, 2019; accepted for publication (in revised form) October 21, 2020; published electronically January 21, 2021.

https://doi.org/10.1137/19M1288280

Funding: The work of the first author was partially supported by National Science Foundation of China under grants 11601468 and 11771375 and by Shandong Province Natural Science Foundation (ZR2018MA008). The work of the second author was partially supported by the U.S. National Science Foundation under grant DMS-1818642. The work of the third author was partially supported by the U.S. National Science Foundation under grants DMS-1720212, DMS-1818783, and DMS-2012490.

†School of Mathematics and Information Sciences, Yantai University, Yantai, 264005, Shandong, P. R. China (gdzhang@ytu.edu.cn).

‡Department of Mathematics, Missouri University of Science & Technology, Rolla, MO 65409 USA (hex@mst.edu).

§Corresponding author. Department of Mathematics, University of South Carolina, Columbia, SC 29208 USA (xfyang@math.sc.edu).

homogeneous monophase fluids. The main difference between these two monophase models is that Rosensweig's model considers the internal rotation of the nanoparticles while Shliomis' model deals with the rotation as a magnetic torque. Recently, some engineering applications arise naturally in the form of two-phase flow, namely, one phase has magnetic properties and the other does not, e.g., magnetic manipulation of microchannel flows, microvalves, magnetically guided transport, etc. In the pioneering work of [33], the authors developed a phase field model for two-phase ferrofluid flows which couples the monophase Shliomis model and the Cahn–Hilliard equations where an artful weighted function is utilized to confine the magnetic field on the ferrofluid phase. Another phase field model for two-phase magnetohydrodynamic flows was also similarly developed in [57]. The model developed in [33] presents the typical benchmarks like the morphology of spikes due to the Rosensweig instability. However, for simplicity in this pioneering work, some nonlinear terms were dropped in [33] such that the challenges of algorithm development and analysis are reduced. Furthermore, it is remarkable that the numerical scheme developed in [33] is nonlinear and fully coupled; thus the implementation of the scheme is relatively complicated with the high computational cost.

In this paper, we first reformulate the two-phase FHD model into a more complete form by restoring all dropped terms and establishing the energy dissipation law. Then, we aim to develop a fully discrete scheme that is not only easy to implement for time discretization (linear and decoupled) and spatial discretization (continuous Galerkin finite element method) but also provably unconditionally energy stable. This is by no means an easy task due to a large number of highly nonlinear couplings among the velocity, pressure, phase variable, magnetization field, and effective magnetizing field through the nontrivial elastic stress tensor, Kelvin force, and fluid convection. To achieve this goal, by combining the projection method for the Navier–Stokes equations, the linear stabilization approach for the double-well potential, the subtle implicit-explicit treatments for nonlinear coupling terms, and some extra stabilization terms, we finally arrive at an efficient fully discrete numerical scheme, and it satisfies the following properties: (i) it is unconditionally stable and satisfies a discrete energy law and (ii) it leads to linear decoupled equations to solve at each time step. To the best of the authors' knowledge, the scheme is the first decoupled, linear, unconditionally energy stable scheme for a phase field model of two-phase ferrofluid flows. We then implement this numerical scheme to conduct the accuracy/stability tests and study dynamic motions of a ferrofluid driven by the Rosensweig instability. Numerical experiments demonstrate the desired accuracy in the time step and spatial grid size, and the presented numerical examples capture some essential phenomenological features of ferrofluid flows.

The rest of the paper is organized as follows. In section 2, we present a two-phase phase field ferrofluid model and derive its energy law. In section 3, we develop a fully discrete finite element numerical scheme and prove its unconditional energy stability rigorously. Various numerical experiments are given in section 4 to show the accuracy and efficiency of the proposed numerical scheme. Finally, some concluding remarks are given in section 5.

2. Two-phase FHD model. We recall that the well-known monophase Shliomis model for a viscous, homogenous, nonconducting ferrofluid flow system confined in a bounded convex polygon/polyhedron $\Omega \subset R^d$ with $d = 2$ or 3 reads as follows [33, 53]:

$$
\begin{cases}
\boldsymbol{u}_t - \nu\Delta\boldsymbol{u} + (\boldsymbol{u}\cdot\nabla)\boldsymbol{u} + \nabla p = \mu(\boldsymbol{m}\cdot\nabla)\boldsymbol{h} + \dfrac{\mu}{2}\nabla\times(\boldsymbol{m}\times\boldsymbol{h}),\\
\nabla\cdot\boldsymbol{u} = 0,\\
\boldsymbol{m}_t + (\boldsymbol{u}\cdot\nabla)\boldsymbol{m} - \dfrac{1}{2}\nabla\times\boldsymbol{u}\times\boldsymbol{m} = -\dfrac{1}{\tau}(\boldsymbol{m} - \chi_0\boldsymbol{h}) - \beta\boldsymbol{m}\times(\boldsymbol{m}\times\boldsymbol{h}),\\
-\Delta\varphi = \nabla\cdot\boldsymbol{m},\\
\boldsymbol{u}|_{\partial\Omega} = 0, \quad \partial_n\varphi|_{\partial\Omega} = (\boldsymbol{h}_a - \boldsymbol{m})\cdot n,\\
\boldsymbol{u}(0,\boldsymbol{x}) = \boldsymbol{u}_0, \quad \boldsymbol{m}(0,\boldsymbol{x}) = \boldsymbol{m}_0,
\end{cases}
\tag{2.1}
$$

where $\boldsymbol{u}$ is the velocity field, p is the pressure, $\boldsymbol{m}$ is magnetization field which expresses the density of induced magnetic dipole moments in a magnetic material, $\boldsymbol{h}(:=\nabla\varphi)$ is the effective magnetizing field, $\boldsymbol{h} = \boldsymbol{h}_a + \boldsymbol{h}_d$ where $\boldsymbol{h}_d$ is the so-called demagnetizing field, $\boldsymbol{h}_a$ is a smooth harmonic applied magnetizing field, and $\nabla\times\boldsymbol{h}_a = \boldsymbol{0}, \nabla\cdot\boldsymbol{h}_a = 0$, ν is the kinematic fluid viscosity, χ_0 is magnetic susceptibility, μ is permeability of free space, τ is relaxation time constant, $\beta = \frac{1}{6\nu\vartheta}$, ϑ is volume fraction of dispersed solid phase, n is the outward normal on the boundary $\partial\Omega$, and the term $(\boldsymbol{m}\cdot\nabla)\boldsymbol{h}$ is the so-called Kelvin force.

We now consider a two-phase FHD phase field model for immiscible mixtures of ferrofluid immersed in a viscous fluid matrix, where the starting point is to extend the above monophase Shliomis model to the two-phase scenario. For the two-phase system (a ferrofluid and its nonferromagnetic viscous medium) with their respective viscosities ν_f and ν_w, using the phase field approach, we introduce a labeling variable Φ as

$$
\Phi(t,\boldsymbol{x}) = \begin{cases} 1 & \text{ferrofluid phase,}\\ 0 & \text{nonmagnetizable viscous medium,}\end{cases}
$$

with a thin smooth transition layer of thickness ϵ connecting the two fluids. Then the interface of the mixture can be described by $\Gamma = \{\boldsymbol{x} : \Phi(t,\boldsymbol{x}) = 1/2\}$. Let $F(\Phi) = \frac{1}{4\epsilon}\Phi^2(\Phi-1)^2$ be the Ginzburg–Landau double-well potential, and define the mixing energy functional as

$$
E_{mix} = \lambda\int_\Omega \Big(\frac{\epsilon}{2}|\nabla\Phi|^2 + F(\Phi)\Big)\,d\boldsymbol{x},
$$

where λ represents the surface tension parameter and the first term (the capillary term) and the second term represent the tendency of hydrophilic and hydrophobic properties, respectively.

By assuming that the evolution of the phase field variable follows the Cahn–Hilliard dynamics (a gradient flow system in H^{-1}), we can derive the following diffusive system:

$$
\begin{cases}
\Phi_t + \nabla\cdot(\boldsymbol{u}\Phi) = M\Delta W,\\
W = -\lambda\epsilon\Delta\Phi + \lambda f(\Phi),\\
\Phi(0,\boldsymbol{x}) = \Phi_0,\\
\partial_n\Phi|_{\partial\Omega} = 0, \quad \partial_n W|_{\partial\Omega} = 0,
\end{cases}
\tag{2.2}
$$

where $M > 0$ is the mobility parameter, W is the chemical potential, and $f(\Phi) = F'(\Phi)$.

In this paper we modify the double-well potential $F(\Phi)$ in order to make its second-order derivative bounded, namely,

$$F(\Phi) = \begin{cases} \frac{1}{4\epsilon}\Phi^2, & \Phi \in (-\infty, 0), \\ \frac{1}{4\epsilon}\Phi^2(\Phi-1)^2, & \Phi \in [0,1], \\ \frac{1}{4\epsilon}(\Phi-1)^2, & \Phi \in (1,+\infty). \end{cases}$$

It is clear that there exists a constant L (e.g., $L = \frac{1}{2\epsilon}$) such that the following boundedness property holds:

$$|f'(\Phi)| = |F''(\Phi)| \le L. \tag{2.3}$$

Remarkably, the magnetization field $\boldsymbol{m}$ is zero for the nonmagnetizable viscous medium; thus $\boldsymbol{m}$ has to be confined only on the ferrofluid region ($\Phi = 1$) instead of the whole domain. To this end, we introduce the magnetic susceptibility function $\chi(\Phi)$ such that $\chi(\Phi) = \chi_0$ in ferrofluid region; $\chi(\Phi) = 0$ otherwise. In this paper, we let $\chi(\Phi) = \chi_0 \frac{1}{1+e^{-(2\Phi-1)/\epsilon}}$ [33] (one can use an alternative choice $\chi(\Phi) = \Phi^2\chi_0$ for simplicity). Since the viscosities of the two fluids differ as well, we assume the viscosity is a function of the phase variable Φ [33], namely,

$$\nu(\Phi) = \nu_w + (\nu_f - \nu_w)\frac{1}{1+e^{-(2\Phi-1)/\epsilon}},$$

where ν_f and ν_w are viscosities for the ferrofluid phase and nonferromagnetic viscous medium, respectively.

By using the above notations, we generalize the monophase case to the two-phase model by combining the Shliomis model (2.1) and Cahn–Hilliard system (2.2). Thus the two-phase ferrofluids system reads as follows:

$$\Phi_t + \nabla\cdot(\boldsymbol{u}\Phi) = M\Delta W, \tag{2.4}$$

$$W = -\lambda\epsilon\Delta\Phi + \lambda f(\Phi), \tag{2.5}$$

$$\boldsymbol{u}_t - \nabla\cdot\nu(\Phi)D(\boldsymbol{u}) + (\boldsymbol{u}\cdot\nabla)\boldsymbol{u} + \nabla p + \Phi\nabla W = \mu(\boldsymbol{m}\cdot\nabla)\boldsymbol{h} + \frac{\mu}{2}\nabla\times(\boldsymbol{m}\times\boldsymbol{h}), \tag{2.6}$$

$$\nabla\cdot\boldsymbol{u} = 0, \tag{2.7}$$

$$\boldsymbol{m}_t + (\boldsymbol{u}\cdot\nabla)\boldsymbol{m} - \frac{1}{2}\nabla\times\boldsymbol{u}\times\boldsymbol{m} + \beta\boldsymbol{m}\times(\boldsymbol{m}\times\boldsymbol{h}) = -\frac{1}{\tau}(\boldsymbol{m} - \chi(\Phi)\boldsymbol{h}), \tag{2.8}$$

$$-\Delta\varphi = \nabla\cdot(\boldsymbol{m} - \boldsymbol{h}_a), \tag{2.9}$$

$$\partial_n\Phi|_{\partial\Omega} = 0, \quad \partial_n W|_{\partial\Omega} = 0, \quad \boldsymbol{u}|_{\partial\Omega} = 0, \quad \partial_n\varphi|_{\partial\Omega} = (\boldsymbol{h}_a - \boldsymbol{m})\cdot n, \tag{2.10}$$

$$\Phi(0,\boldsymbol{x}) = \Phi_0, \quad \boldsymbol{u}(0,\boldsymbol{x}) = \boldsymbol{u}_0, \quad \boldsymbol{m}(0,\boldsymbol{x}) = \boldsymbol{m}_0, \tag{2.11}$$

where $D(\boldsymbol{u}) = \frac{1}{2}(\nabla\boldsymbol{u} + \nabla\boldsymbol{u}^T)$ and the term $\Phi\nabla W$ is the induced elastic stress by the mixing energy [33, 49, 50, 51, 60].

Remark 2.1. We remark that this model is consistent with the monophase case (2.1) when $\Phi \equiv 1$. When $\Phi = 0$, we take the L^2 inner product of (2.8) with $\boldsymbol{m}$ to get

$$\frac{1}{2}\frac{d}{dt}\|\boldsymbol{m}\|^2 + \frac{1}{\tau}\|\boldsymbol{m}\|^2 = 0,$$

where we use $((\boldsymbol{u}\cdot\nabla)\boldsymbol{m}, \boldsymbol{m}) = 0$, $(\nabla\times\boldsymbol{u}\times\boldsymbol{m}, \boldsymbol{m}) = 0$, and $(\boldsymbol{m}\times(\boldsymbol{m}\times\boldsymbol{h}), \boldsymbol{m}) = 0$. Taking integration of above equation in time, we have

$$\frac{1}{2}\|\boldsymbol{m}(t)\|^2 - \frac{1}{2}\|\boldsymbol{m}(0)\|^2 + \frac{1}{\tau}\int_0^t \|\boldsymbol{m}(s)\|^2 ds = 0.$$

Therefore, we derive the magnetization field $\boldsymbol{m} = 0$ in the nonferrofluid phase only if $\boldsymbol{m}|_{t=0} = 0$ in the nonferrofluid phase.

To show the two-phase FHD model (2.4)–(2.11) follows the energy law, we need the following lemma.

LEMMA 2.1. *Suppose* $\boldsymbol{m}, \boldsymbol{u} \in L^2(\Omega)^d$, $\boldsymbol{h} \in H^1(\Omega)^d$, $d = 2, 3$; *there holds the identity*

$$((\boldsymbol{m} \cdot \nabla)\boldsymbol{h}, \boldsymbol{u}) + (\boldsymbol{u} \times \boldsymbol{m}, \nabla \times \boldsymbol{h}) = ((\boldsymbol{u} \cdot \nabla)\boldsymbol{h}, \boldsymbol{m}). \tag{2.12}$$

Proof. For two dimensions with $d = 2$, we obtain the following identity by some simple calculations:

$$\begin{aligned}((\boldsymbol{u} \cdot \nabla)\boldsymbol{h}, \boldsymbol{m}) - ((\boldsymbol{m} \cdot \nabla)\boldsymbol{h}, \boldsymbol{u}) &= \int_\Omega \left(\frac{\partial h_1}{\partial y} - \frac{\partial h_2}{\partial x}\right)(u_2 m_1 - u_1 m_2) d\boldsymbol{x} \\ &= (\boldsymbol{u} \times \boldsymbol{m}, \nabla \times \boldsymbol{h}).\end{aligned}$$

Similarly, for three dimensions with $d = 3$, we derive

$$\begin{aligned}&((\boldsymbol{u} \cdot \nabla)\boldsymbol{h}, \boldsymbol{m}) - ((\boldsymbol{m} \cdot \nabla)\boldsymbol{h}, \boldsymbol{u}) \\ &\quad = \int_\Omega \left(\frac{\partial h_1}{\partial y} - \frac{\partial h_2}{\partial x}\right)(u_2 m_1 - u_1 m_2) + \left(\frac{\partial h_1}{\partial z} - \frac{\partial h_3}{\partial x}\right)(u_3 m_1 - u_1 m_3) \\ &\qquad + \left(\frac{\partial h_2}{\partial z} - \frac{\partial h_3}{\partial y}\right)(u_3 m_2 - u_2 m_3) d\boldsymbol{x} \\ &\quad = (\boldsymbol{u} \times \boldsymbol{m}, \nabla \times \boldsymbol{h}).\end{aligned}$$

The proof is complete. ∎

The two-phase FHD system (2.4)–(2.11) satisfies the following energy law.

THEOREM 2.1. *Assuming* $\chi(\Phi) \le \chi_0$, *the system* (2.4)–(2.11) *satisfies the following energy law in the sense that*

$$\frac{d}{dt} E(\Phi, \boldsymbol{u}, \boldsymbol{h}, \boldsymbol{m}) + D(W, \boldsymbol{u}, \boldsymbol{h}, \boldsymbol{m}) \le \frac{\mu}{\tau} \|\boldsymbol{h}_a\|^2 + \tau\mu \|(\boldsymbol{h}_a)_t\|^2,$$

where

$$\begin{aligned}E(\Phi, \boldsymbol{u}, \boldsymbol{h}, \boldsymbol{m}) &= \lambda\Big(\frac{\epsilon}{2}\|\nabla\Phi\|^2 + (F(\Phi), 1)\Big) + \frac{1}{2}\|\boldsymbol{u}\|^2 + \frac{\mu}{2}\|\boldsymbol{h}\|^2 + \frac{\mu}{2\chi_0}\|\boldsymbol{m}\|^2, \\ D(W, \boldsymbol{u}, \boldsymbol{h}, \boldsymbol{m}) &= M\|\nabla W\|^2 + \|\sqrt{\nu(\Phi)} D(\boldsymbol{u})\|^2 \\ &\qquad + \frac{\mu}{2\tau}\|\boldsymbol{h}\|^2 + \mu\beta\|\boldsymbol{m} \times \boldsymbol{h}\|^2 + \frac{3\mu}{4\tau\chi_0}\|\boldsymbol{m}\|^2.\end{aligned}$$

Proof. By taking the L^2 inner product of (2.4) with W and applying integration by parts, we obtain

$$(\Phi_t, W) - (\boldsymbol{u}\Phi, \nabla W) = -M\|\nabla W\|^2. \tag{2.13}$$

By taking the L^2 inner product of (2.5) with $-\Phi_t$, we derive

$$-(W, \Phi_t) = -\lambda \frac{d}{dt}\Big(\frac{\epsilon}{2}\|\nabla\Phi\|^2 + (F(\Phi), 1)\Big). \tag{2.14}$$

By taking the L^2 inner product of (2.6) with $\boldsymbol{u}$, we derive

$$\frac{1}{2}\frac{d}{dt}\|\boldsymbol{u}\|^2 + \|\sqrt{\nu(\Phi)}D(\boldsymbol{u})\|^2 + (\Phi\nabla W, \boldsymbol{u}) = \mu((\boldsymbol{m}\cdot\nabla)\boldsymbol{h}, \boldsymbol{u}) + \frac{\mu}{2}(\boldsymbol{m}\times\boldsymbol{h}, \nabla\times\boldsymbol{u}). \tag{2.15}$$

By taking the L^2 inner product of (2.8) with $\mu\boldsymbol{h}$, we get

$$\begin{aligned}\frac{\mu}{\tau}\|\sqrt{\chi(\Phi)}\boldsymbol{h}\|^2 + \mu\beta\|\boldsymbol{m}\times\boldsymbol{h}\|^2 - \mu(\boldsymbol{m}_t, \boldsymbol{h}) - \frac{\mu}{\tau}(\boldsymbol{m}, \boldsymbol{h})\\ = \mu((\boldsymbol{u}\cdot\nabla)\boldsymbol{m}, \boldsymbol{h}) - \frac{\mu}{2}(\nabla\times\boldsymbol{u}\times\boldsymbol{m}, \boldsymbol{h}).\end{aligned} \tag{2.16}$$

By taking the L^2 inner product of (2.9) with $\frac{\mu}{\tau}\varphi$, we get

$$\frac{\mu}{\tau}\|\nabla\varphi\|^2 + \frac{\mu}{\tau}(\boldsymbol{m}, \nabla\varphi) = \frac{\mu}{\tau}(\boldsymbol{h}_a, \nabla\varphi). \tag{2.17}$$

By taking the time derivative of (2.9) and taking the L^2 inner product of it with $\mu\varphi$, we get

$$\frac{d}{dt}\left(\frac{\mu}{2}\|\nabla\varphi\|^2\right) + \mu(\boldsymbol{m}_t, \nabla\varphi) = \mu((\boldsymbol{h}_a)_t, \nabla\varphi). \tag{2.18}$$

From Lemma 2.1 and noting that $\nabla\times\boldsymbol{h} = \nabla\times\nabla\varphi = 0$, we derive

$$\begin{aligned}((\boldsymbol{m}\cdot\nabla)\boldsymbol{h}, \boldsymbol{u}) + ((\boldsymbol{u}\cdot\nabla)\boldsymbol{m}, \boldsymbol{h}) &= ((\boldsymbol{u}\cdot\nabla)\boldsymbol{h}, \boldsymbol{m}) - (\boldsymbol{u}\times\boldsymbol{m}, \nabla\times\boldsymbol{h}) + ((\boldsymbol{u}\cdot\nabla)\boldsymbol{m}, \boldsymbol{h})\\ &= ((\boldsymbol{u}\cdot\nabla)\boldsymbol{h}, \boldsymbol{m}) + ((\boldsymbol{u}\cdot\nabla)\boldsymbol{m}, \boldsymbol{h})\\ &= 0,\end{aligned} \tag{2.19}$$

where the last equality holds since $\boldsymbol{u}$ is divergence free and $\boldsymbol{u}\cdot n|_{\partial\Omega} = 0$ (see also Lemma 3.1 in [33]).

Therefore, by combining (2.13)–(2.18), using (2.19) and $\boldsymbol{h} = \nabla\varphi$, we obtain

$$\begin{aligned}&\frac{d}{dt}\left(\lambda\left(\frac{\epsilon}{2}\|\nabla\Phi\|^2 + (F(\Phi), 1)\right) + \frac{1}{2}\|\boldsymbol{u}\|^2 + \frac{\mu}{2}\|\boldsymbol{h}\|^2\right)\\ &\qquad + M\|\nabla W\|^2 + \|\sqrt{\nu(\Phi)}D(\boldsymbol{u})\|^2 + \frac{\mu}{\tau}\|\sqrt{\chi(\Phi)}\boldsymbol{h}\|^2\\ &\qquad + \frac{\mu}{\tau}\|\boldsymbol{h}\|^2 + \mu\beta\|\boldsymbol{m}\times\boldsymbol{h}\|^2\\ &= \frac{\mu}{\tau}(\boldsymbol{h}_a, \boldsymbol{h}) + \mu((\boldsymbol{h}_a)_t, \boldsymbol{h}).\end{aligned} \tag{2.20}$$

Furthermore, by taking the L^2 inner product of (2.8) with $\frac{\mu}{\chi_0}\boldsymbol{m}$, we get

$$\frac{d}{dt}\left(\frac{\mu}{2\chi_0}\|\boldsymbol{m}\|^2\right) + \frac{\mu}{\tau\chi_0}\|\boldsymbol{m}\|^2 = \frac{\mu}{\tau\chi_0}(\chi(\Phi)\boldsymbol{h}, \boldsymbol{m}), \tag{2.21}$$

where we use following three identities:

$$\begin{aligned}&(\nabla\times\boldsymbol{u}\times\boldsymbol{m}, \boldsymbol{m}) = 0,\\ &(\boldsymbol{m}\times(\boldsymbol{m}\times\boldsymbol{h}), \boldsymbol{m}) = 0,\\ &((\boldsymbol{u}\cdot\nabla)\boldsymbol{m}, \boldsymbol{m}) = 0 \text{ if } \nabla\cdot\boldsymbol{u} = 0, \boldsymbol{u}\cdot n|_{\partial\Omega} = 0.\end{aligned} \tag{2.22}$$

By combining (2.20) with (2.21), we derive

$$\begin{aligned}
&\frac{d}{dt}\left(\lambda\left(\frac{\epsilon}{2}\|\nabla\Phi\|^2+(F(\Phi),1)\right)+\frac{1}{2}\|\boldsymbol{u}\|^2+\frac{\mu}{2}\|\boldsymbol{h}\|^2+\frac{\mu}{2\chi_0}\|\boldsymbol{m}\|^2\right)\\
&\quad+M\|\nabla W\|^2+\|\sqrt{\nu(\Phi)}D(\boldsymbol{u})\|^2+\frac{\mu}{\tau}\|\sqrt{\chi(\Phi)}\boldsymbol{h}\|^2\\
&\quad+\frac{\mu}{\tau}\|\boldsymbol{h}\|^2+\mu\beta\|\boldsymbol{m}\times\boldsymbol{h}\|^2+\frac{\mu}{\tau\chi_0}\|\boldsymbol{m}\|^2\\
&\quad=\frac{\mu}{\tau}(\boldsymbol{h}_a,\boldsymbol{h})+\mu((\boldsymbol{h}_a)_t,\boldsymbol{h})+\frac{\mu}{\tau\chi_0}(\chi(\Phi)\boldsymbol{h},\boldsymbol{m}). \qquad (2.23)
\end{aligned}$$

We estimate the term on the right-hand side by

$$\begin{aligned}
\frac{\mu}{\tau\chi_0}(\chi(\Phi)\boldsymbol{h},\boldsymbol{m})&\le\frac{\mu}{\tau\chi_0}\|\sqrt{\chi(\Phi)}\boldsymbol{h}\|\|\sqrt{\chi(\Phi)}\boldsymbol{m}\|\le\frac{\mu}{\tau}\|\sqrt{\chi(\Phi)}\boldsymbol{h}\|^2+\frac{\mu}{4\tau\chi_0^2}\|\sqrt{\chi(\Phi)}\boldsymbol{m}\|^2\\
&\le\frac{\mu}{\tau}\|\sqrt{\chi(\Phi)}\boldsymbol{h}\|^2+\frac{\mu}{4\tau\chi_0^2}\chi_0\|\boldsymbol{m}\|^2 \qquad (2.24)\\
&=\frac{\mu}{\tau}\|\sqrt{\chi(\Phi)}\boldsymbol{h}\|^2+\frac{\mu}{4\tau\chi_0}\|\boldsymbol{m}\|^2,
\end{aligned}$$

$$\frac{\mu}{\tau}(\boldsymbol{h}_a,\boldsymbol{h})\le\frac{\mu}{\tau}\|\boldsymbol{h}_a\|\|\boldsymbol{h}\|\le\frac{\mu}{4\tau}\|\boldsymbol{h}\|^2+\frac{\mu}{\tau}\|\boldsymbol{h}_a\|^2, \qquad (2.25)$$

$$\mu((\boldsymbol{h}_a)_t,\boldsymbol{h})\le\mu\|(\boldsymbol{h}_a)_t\|\|\boldsymbol{h}\|\le\frac{\mu}{4\tau}\|\boldsymbol{h}\|^2+\tau\mu\|(\boldsymbol{h}_a)_t\|^2. \qquad (2.26)$$

Finally, by combining (2.23) with (2.24)–(2.26), we arrive at

$$\begin{aligned}
&\frac{d}{dt}E(\Phi,\boldsymbol{u},\boldsymbol{h},\boldsymbol{m})+M\|\nabla W\|^2+\|\sqrt{\nu(\Phi)}D(\boldsymbol{u})\|^2+\frac{\mu}{2\tau}\|\boldsymbol{h}\|^2+\mu\beta\|\boldsymbol{m}\times\boldsymbol{h}\|^2+\frac{3\mu}{4\tau\chi_0}\|\boldsymbol{m}\|^2\\
&\quad\le\frac{\mu}{\tau}\|\boldsymbol{h}_a\|^2+\tau\mu\|(\boldsymbol{h}_a)_t\|^2, \qquad (2.27)
\end{aligned}$$

which completes the proof. ∎

Remark 2.2. For comparisons, we present the two-phase FHD model given in [33] that reads as

$$\begin{cases}
\Phi_t+\nabla\cdot(\boldsymbol{u}\Phi)=M\Delta W,\\
W=-\lambda\epsilon\Delta\Phi+\lambda f(\Phi),\\
\boldsymbol{u}_t-\nabla\cdot\nu(\Phi)D(\boldsymbol{u})+(\boldsymbol{u}\cdot\nabla)\boldsymbol{u}+\nabla p+\Phi\nabla W=\mu(\boldsymbol{m}\cdot\nabla)\boldsymbol{h},\\
\nabla\cdot\boldsymbol{u}=0,\\
\boldsymbol{m}_t+(\boldsymbol{u}\cdot\nabla)\boldsymbol{m}=-\dfrac{1}{\tau}\left(\boldsymbol{m}-\chi(\Phi)\boldsymbol{h}\right),\\
-\Delta\varphi=\nabla\cdot(\boldsymbol{m}-\boldsymbol{h}_a).
\end{cases} \qquad (2.28)$$

One can see that the model (2.28) actually dropped one term in the momentum equation ($\frac{\mu}{2}\nabla\times(\boldsymbol{m}\times\boldsymbol{h})$) and two terms in the magnetization field equation ($-\frac{1}{2}\nabla\times\boldsymbol{u}\times\boldsymbol{m}$ and $\beta\boldsymbol{m}\times(\boldsymbol{m}\times\boldsymbol{h})$) which may somewhat reduce the difficulties of algorithm development. Meanwhile, the dissipative law obtained in [33] requests an extra condition on χ_0 ($\chi_0\le 4$) which is apparently not needed in our proof.

3. Numerical scheme. To solve the two-phase FHD model (2.4)–(2.11), by discretizing the space using the continuous Galerkin finite element method, we develop an efficient scheme that is linear, decoupled, unconditionally energy stable, and first-order accurate in time.

Let $N > 0$ to denote the total number of time steps, define the uniform time step size as $\delta t = [\frac{T}{N}]$, and set $t_n = n\delta t$. We also define the backward difference operator d_t as $d_t\psi^n = \frac{\psi^n - \psi^{n-1}}{\delta t}$ for any variable ψ.

We introduce a series of finite-dimensional discrete subspaces:

$$Y_h \subset H^1(\Omega), \boldsymbol{V}_h \subset H_0^1(\Omega)^d, Q_h \subset L_0^2(\Omega), \boldsymbol{N}_h \subset L^2(\Omega)^d, \Psi_h \subset H^1(\Omega) \cap L_0^2(\Omega). \tag{3.1}$$

Here the $L_0^2(\Omega) = \{q \in L^2(\Omega) : \int_\Omega q dx = 0\}$. The semidiscrete formulations of the system (2.4)–(2.11) in the weak form reads as follows: find $(\Phi, W, \boldsymbol{u}, p, \boldsymbol{m}, \varphi) \in Y_h \times Y_h \times \boldsymbol{V}_h \times Q_h \times \boldsymbol{N}_h \times \Psi_h$ such that for $(\Lambda, X, \boldsymbol{v}, q, \boldsymbol{n}, \psi) \in Y_h \times Y_h \times \boldsymbol{V}_h \times Q_h \times \boldsymbol{N}_h \times \Psi_h$,

$$\begin{cases} (\Phi_t, \Lambda) - (\boldsymbol{u}\Phi, \nabla\Lambda) = -M(\nabla W, \nabla\Lambda), \\ (W, X) = \lambda\epsilon(\nabla\Phi, \nabla X) + \lambda(f(\Phi), X), \\ (\boldsymbol{u}_t, \boldsymbol{v}) + (\nu(\Phi)D(\boldsymbol{u}), D(\boldsymbol{v})) + (B(\boldsymbol{u}, \boldsymbol{u}), \boldsymbol{v}) - (p, \nabla\cdot\boldsymbol{v}) + (\Phi\nabla W, \boldsymbol{v}) \\ \qquad\qquad = \mu((\boldsymbol{m}\cdot\nabla)\boldsymbol{h}, \boldsymbol{v}) + \dfrac{\mu}{2}(\boldsymbol{m}\times\boldsymbol{h}, \nabla\times\boldsymbol{v}), \\ (\nabla\cdot\boldsymbol{u}, q) = 0, \\ (\boldsymbol{m}_t, \boldsymbol{n}) + ((\boldsymbol{u}\cdot\nabla)\boldsymbol{m}, \boldsymbol{n}) - \dfrac{1}{2}(\nabla\times\boldsymbol{u}\times\boldsymbol{m}, \boldsymbol{n}) - \beta(\boldsymbol{m}\times\boldsymbol{h}, \boldsymbol{m}\times\boldsymbol{n}) \\ \qquad\qquad = -\dfrac{1}{\tau}(\boldsymbol{m}, \boldsymbol{n}) + \dfrac{1}{\tau}(\chi(\Phi)\boldsymbol{h}, \boldsymbol{n}), \\ (\nabla\varphi, \nabla\psi) = -(\boldsymbol{m}, \nabla\psi) + (\boldsymbol{h}_a, \nabla\psi), \end{cases} \tag{3.2}$$

where the bilinear form $B(\boldsymbol{u}, \boldsymbol{v})$ is defined as

$$B(\boldsymbol{u}, \boldsymbol{v}) := (\boldsymbol{u}\cdot\nabla)\boldsymbol{v} + \frac{1}{2}(\nabla\cdot\boldsymbol{u})\boldsymbol{v}. \tag{3.3}$$

Remark 3.1. $B(\boldsymbol{u}, \boldsymbol{v})$ is the skew-symmetric form of the nonlinear convective terms. If the velocity is divergence free, then $B(\boldsymbol{u}, \boldsymbol{v}) = (\boldsymbol{u}\cdot\nabla)\boldsymbol{v}$ and $B(\boldsymbol{u}, \boldsymbol{m}) = (\boldsymbol{u}\cdot\nabla)\boldsymbol{m}$. We define a trilinear form as

$$b(\boldsymbol{u}, \boldsymbol{v}, \boldsymbol{w}) = (B(\boldsymbol{u}, \boldsymbol{v}), \boldsymbol{w}) = ((\boldsymbol{u}\cdot\nabla)\boldsymbol{v}, \boldsymbol{w}) + \frac{1}{2}((\nabla\cdot\boldsymbol{u})\boldsymbol{v}, \boldsymbol{w}).$$

In the numerical scheme, the velocity may not be divergence free, but notice the following identity:

$$b(\boldsymbol{u}, \boldsymbol{v}, \boldsymbol{v}) = (B(\boldsymbol{u}, \boldsymbol{v}), \boldsymbol{v}) = 0 \,\text{if}\, \boldsymbol{u}\cdot n|_{\partial\Omega} = 0. \tag{3.4}$$

In other words, this identity holds regardless of whether $\boldsymbol{u}$ or $\boldsymbol{v}$ are divergence free or not, which would help to preserve the discrete energy stability. Meanwhile, through some basic calculations, for $\boldsymbol{u} \in H_0^1(\Omega)^d$, $\boldsymbol{v}, \boldsymbol{w} \in H^1(\Omega)^d$, the following identity also holds:

$$b(\boldsymbol{u}, \boldsymbol{v}, \boldsymbol{w}) = \frac{1}{2}((\boldsymbol{u}\cdot\nabla)\boldsymbol{v}, \boldsymbol{w}) - \frac{1}{2}((\boldsymbol{u}\cdot\nabla)\boldsymbol{w}, \boldsymbol{v}). \tag{3.5}$$

Assuming that the polygonal/polyhedral domain Ω is discretized by a conforming and shape regular triangulation/tetrahedron mesh $\mathcal{T}_h$ that is composed by open disjoint elements K such that $\bar{\Omega} = \bigcup_{K\in\mathcal{T}_h} \bar{K}$, we use $\mathcal{P}_l$ to denote the space of polynomials of total degree at most l and define the following finite element spaces:

$$
\begin{aligned}
Y_h &= \left\{X \in C^0(\Omega) : X|_K \in \mathcal{P}_{l_1}(K)\ \forall K \in \mathcal{T}_h\right\},\\
\boldsymbol{V}_h &= \left\{\boldsymbol{v} \in C^0(\Omega)^d : \boldsymbol{v}|_K \in \mathcal{P}_{l_2}(K)^d\ \forall K \in \mathcal{T}_h\right\} \cap H_0^1(\Omega)^d,\\
Q_h &= \left\{q \in C^0(\Omega) : q|_K \in \mathcal{P}_{l_2-1}(K)\ \forall K \in \mathcal{T}_h\right\} \cap L_0^2(\Omega),\\
\boldsymbol{N}_h &= \left\{\boldsymbol{n} \in C^0(\Omega)^d : \boldsymbol{n}|_K \in \mathcal{P}_{l_3-1}(K)^d\ \forall K \in \mathcal{T}_h\right\},\\
\Psi_h &= \left\{\psi \in C^0(\Omega) : \psi|_K \in \mathcal{P}_{l_3}(K)\ \forall K \in \mathcal{T}_h\right\} \cap L_0^2(\Omega).
\end{aligned}
\tag{3.6}
$$

Besides, we assume the pair of spaces $(\boldsymbol{V}_h, Q_h)$ satisfy the *inf-sup* condition [20]:

$$
\beta\|q\| \le \sup_{\boldsymbol{v}\in\boldsymbol{V}_h} \frac{(\nabla\cdot\boldsymbol{v}, q)}{\|\nabla\boldsymbol{v}\|} \quad \forall q \in Q_h,
$$

where the constant β only depends on Ω. A well-known *inf-sup* stable pair $(\boldsymbol{V}_h, Q_h)$ is the Taylor–Hood element [20].

Our numerical scheme reads as follows.

Initially, given $\boldsymbol{m}^0$ and $\boldsymbol{h}_a^0$, we find $\varphi^0 \in \Psi_h$ such that

$$
(\nabla\varphi^0, \nabla\psi) = -(\boldsymbol{m}^0, \nabla\psi) + (\boldsymbol{h}_a^0, \nabla\psi)\ \forall\psi \in \Psi_h \tag{3.7}
$$

and $\tilde{\boldsymbol{h}}^0 \in \boldsymbol{N}_h$ such that

$$
(\tilde{\boldsymbol{h}}^0, \boldsymbol{Z}) = (\nabla\varphi^0, \boldsymbol{Z})\ \forall\boldsymbol{Z} \in \boldsymbol{N}_h. \tag{3.8}
$$

Step 1. Find $(\Phi^n, W^n) \in Y_h \times Y_h$ such that for all $(\Lambda, X) \in Y_h \times Y_h$,

$$
(d_t\Phi^n, \Lambda) - (\boldsymbol{u}^{n-1}\Phi^{n-1}, \nabla\Lambda) + \frac{\delta t}{2}(\Phi^{n-1}\nabla W^n, \Phi^{n-1}\nabla\Lambda) + M(\nabla W^n, \nabla\Lambda) = 0, \tag{3.9}
$$

$$
(W^n, X) = \lambda\epsilon(\nabla\Phi^n, \nabla X) + S(\Phi^n - \Phi^{n-1}, X) + \lambda(f(\Phi^{n-1}), X). \tag{3.10}
$$

Step 2. Find $\tilde{\boldsymbol{u}}^n \in \boldsymbol{V}_h$ such that for all $\boldsymbol{v} \in \boldsymbol{V}_h$,

$$
\begin{aligned}
\left(\frac{\tilde{\boldsymbol{u}}^n - \boldsymbol{u}^{n-1}}{\delta t}, \boldsymbol{v}\right) &+ (\nu(\Phi^n)D(\tilde{\boldsymbol{u}}^n), D(\boldsymbol{v})) + b(\boldsymbol{u}^{n-1}, \tilde{\boldsymbol{u}}^n, \boldsymbol{v}) - (p^{n-1}, \nabla\cdot\boldsymbol{v})\\
&+ b_{stab}(\boldsymbol{m}^{n-1}, \tilde{\boldsymbol{u}}^n, \boldsymbol{v}) + (\Phi^{n-1}\nabla W^n, \boldsymbol{v})\\
&= \mu((\boldsymbol{m}^{n-1}\cdot\nabla)\tilde{\boldsymbol{h}}^{n-1}, \boldsymbol{v}) + \frac{\mu}{2}(\boldsymbol{m}^{n-1}\times\tilde{\boldsymbol{h}}^{n-1}, \nabla\times\boldsymbol{v})\\
&+ \mu(\boldsymbol{m}^{n-1}\times\nabla\times\tilde{\boldsymbol{h}}^{n-1}, \boldsymbol{v}),
\end{aligned}
\tag{3.11}
$$

where b_{stab} includes three extra first-order stabilization terms that read as

$$
\begin{aligned}
b_{stab}(\boldsymbol{m}^{n-1}, \tilde{\boldsymbol{u}}^n, \boldsymbol{v}) = {}& \mu\delta t((\tilde{\boldsymbol{u}}^n\cdot\nabla)\boldsymbol{m}^{n-1}, (\boldsymbol{v}\cdot\nabla)\boldsymbol{m}^{n-1})\\
&+ 2\mu\delta t\left((\nabla\cdot\tilde{\boldsymbol{u}}^n)\boldsymbol{m}^{n-1}, (\nabla\cdot\boldsymbol{v})\boldsymbol{m}^{n-1}\right)\\
&+ \frac{\mu}{2}\delta t(\boldsymbol{m}^{n-1}\times\nabla\times\tilde{\boldsymbol{u}}^n, \boldsymbol{m}^{n-1}\times\nabla\times\boldsymbol{v}).
\end{aligned}
$$

Step 3. Find $p^n \in Q_h$ such that for all $q \in Q_h$,

$$(\nabla p^n, \nabla q) = -\frac{1}{\delta t}(\nabla \cdot \tilde{\boldsymbol{u}}^n, q) + (\nabla p^{n-1}, \nabla q). \tag{3.12}$$

Step 4. Update $\boldsymbol{u}^n$ from

$$\boldsymbol{u}^n = \tilde{\boldsymbol{u}}^n - \delta t \nabla p^n + \delta t \nabla p^{n-1}. \tag{3.13}$$

Step 5. Find $(\tilde{\boldsymbol{m}}^n, \varphi^n, \tilde{\boldsymbol{h}}^n) \in \boldsymbol{N}_h \times \Psi_h \times \boldsymbol{N}_h$ such that for all $(\boldsymbol{n}, \psi, \boldsymbol{Z}) \in \boldsymbol{N}_h \times \Psi_h \times \boldsymbol{N}_h$,

$$\begin{aligned}(d_t\tilde{\boldsymbol{m}}^n, \boldsymbol{n}) + ((\tilde{\boldsymbol{u}}^n \cdot \nabla)\boldsymbol{m}^{n-1}, \boldsymbol{n}) + ((\nabla \cdot \tilde{\boldsymbol{u}}^n)\boldsymbol{m}^{n-1}, \boldsymbol{n}) - \frac{1}{2}(\nabla \times \tilde{\boldsymbol{u}}^n \times \boldsymbol{m}^{n-1}, \boldsymbol{n}) \\ = -\frac{1}{\tau}(\tilde{\boldsymbol{m}}^n, \boldsymbol{n}) + \frac{1}{\tau}(\chi(\Phi^n)\tilde{\boldsymbol{h}}^n, \boldsymbol{n}) + \beta(\boldsymbol{m}^{n-1} \times \tilde{\boldsymbol{h}}^n, \boldsymbol{m}^{n-1} \times \boldsymbol{n}),\end{aligned} \tag{3.14}$$

$$(\nabla \varphi^n, \nabla \psi) = -(\tilde{\boldsymbol{m}}^n, \nabla \psi) + (\boldsymbol{h}_a^n, \nabla \psi), \tag{3.15}$$

$$(\tilde{\boldsymbol{h}}^n, \boldsymbol{Z}) = (\nabla \varphi^n, \boldsymbol{Z}). \tag{3.16}$$

Step 6. Set $\boldsymbol{h}^n = \nabla \varphi^n$, and find $\boldsymbol{m}^n \in \boldsymbol{N}_h$ such that for $\boldsymbol{n} \in \boldsymbol{N}_h$,

$$\begin{aligned}(d_t\boldsymbol{m}^n, \boldsymbol{n}) + b(\tilde{\boldsymbol{u}}^n, \boldsymbol{m}^n, \boldsymbol{n}) - \frac{1}{2}(\nabla \times \boldsymbol{u}^n \times \boldsymbol{m}^n, \boldsymbol{n}) \\ = -\frac{1}{\tau}(\boldsymbol{m}^n, \boldsymbol{n}) + \frac{1}{\tau}(\chi(\Phi^n)\tilde{\boldsymbol{h}}^n, \boldsymbol{n}) + \beta(\boldsymbol{m}^{n-1} \times \boldsymbol{h}^n, \boldsymbol{m}^n \times \boldsymbol{n}).\end{aligned} \tag{3.17}$$

Several remarks are in order.

Remark 3.2. There exist a couple of substantial numerical challenges to develop the fully discrete scheme with unconditional energy stability for the FHD model (2.4)–(2.11). First, we recall that two test functions, $\boldsymbol{h}$ and $\boldsymbol{m}$, are needed to be taken for (2.8) in the proof of Theorem 2.1. It is well known that the proof of the discrete energy law for a numerical scheme usually follows the same lines of the energy law for the PDE system. Therefore, for the discrete scheme, two test functions, $\boldsymbol{h}^n$ and $\boldsymbol{m}^n$, are needed to be taken as well if we follow a similar procedure. This naturally brings up a dilemma that both the variables $\boldsymbol{h}$ and $\boldsymbol{m}$ have to be treated in the implicit way, which leads to a fully coupled nonlinear scheme with the high computational cost. Second, the definition of $\boldsymbol{h} = \nabla\varphi$ implies that one has to adopt the hybrid finite element method, e.g., the discontinuous Galerkin method for $\boldsymbol{h}$ and continuous Galerkin method for φ in [33, 34] which is not easy to implement as well.

These two difficulties are overcome by introducing two auxiliary intermediate variables $\tilde{\boldsymbol{m}}^n$ and $\tilde{\boldsymbol{h}}^n$ in Step 5 that is briefly described as follows.

- First, instead of taking the L^2 inner product of $\boldsymbol{h}$ and $\boldsymbol{m}$ within the same equation, we solve the intermediate variable $\tilde{\boldsymbol{m}}^n$ by (3.14) first and then solve the final solution $\boldsymbol{m}^n$ by (3.17). Therefore, in the stability proof, we take the L^2 inner product of (3.14) with $\tilde{\boldsymbol{h}}^n$, and of (3.17) with $\boldsymbol{m}^n$, respectively, which leads to a linear scheme in turn. Moreover, for the convective term, in (3.17), we use the trilinear form $b(\boldsymbol{u}, \boldsymbol{m}, \boldsymbol{n})$. But in (3.14), we still use $((\boldsymbol{u} \cdot \nabla)\boldsymbol{m}, \boldsymbol{n})$ but add an extra consistent term $((\nabla \cdot \boldsymbol{u})\boldsymbol{m}, \boldsymbol{n})$ (a zero term at the continuous case) which plays the key role to obtain the energy stability.
- Second, the intermediate variable $\tilde{\boldsymbol{h}}^n$ is actually the L^2 projection of $\nabla\varphi^n$. Thus both $\boldsymbol{h}$ and φ could be treated by using the continuous Galerkin method.

However, the usage of these two intermediate variables brings up another disadvantage, i.e., the term $\nabla\times\tilde{\boldsymbol{h}}^n$ might not be equal to zero, rigorously. Thus, to obtain the unconditional energy stability, we add an extra consistent term $\boldsymbol{m}\times\nabla\times\boldsymbol{h}$ (a zero term at the continuous case) in the momentum equation, which helps to hold the desired skew-symmetric property even though $\nabla\times\tilde{\boldsymbol{h}}^n\neq 0$ using Lemma 2.1.

Remark 3.3. We discretize the cubic nonlinear term $f(\Phi)$ by the so-called stabilized explicit method [49], where $f(\Phi)$ is discretized explicitly and an extra first-order stabilizer (associated with S) is added in the scheme. The error that this term introduces is of the order $S\delta t\phi_t(\cdot)$, that is, of the same order as the error introduced by the first-order explicit approach of the nonlinear term $f(\Phi)$. It is worth mentioning that there exist many successful techniques to discretize the nonlinear potential to obtain energy stable schemes for the Cahn–Hilliard equation, for instance, the convex-splitting method [13, 14, 16, 28, 43, 46, 55, 66], the implicit quadrature method [22], the invariant energy quadratization method [11, 56, 58, 59, 61, 62, 63, 64], the scalar auxiliary variable method [12, 29, 47, 48], etc. A comparison between the numerical simulation results and lab experiment results was also provided in [6]. Note that we can easily incorporate these methods in (3.9) to discretize $f(\Phi)$. Since the main difficulty to develop energy stable scheme of the two-phase FHD system is how to discretize the coupled nonlinear terms, we choose the stabilized explicit method in this paper due to its simplicity for multiphysics problems [19].

Remark 3.4. The computation of $\boldsymbol{u}$ and p is decoupled by using the pressure-correction method (a typical kind of projection method); see also [23, 24, 25, 37, 39, 44, 45]. The final solution $\boldsymbol{u}^n$ satisfies the discrete divergence free condition which can be deduced by taking the L^2 inner product of (3.13)) with ∇q, $q\in Q_h$,

$$(\boldsymbol{u}^n,\nabla q)=-(\nabla\cdot\tilde{\boldsymbol{u}}^n,q)-\delta t(\nabla(p^n-p^{n-1}),\nabla q). \tag{3.18}$$

This implies $(\boldsymbol{u}^n,\nabla q)=0$ from (3.12).

Remark 3.5. In (3.9), inspired by [7] which deals with the three-phase flow and [50] which deals with the two-phase complex fluids, we add an explicit stabilization term $\frac{\delta t}{2}(\Phi^{n-1}\nabla W^n,\Phi^{n-1}\nabla\Lambda)$to decouple the computations of (Φ,W) and $\boldsymbol{u}$. Moreover, three extra first-order stabilization terms are added in (3.11) (the terms in b_{stab}) that play the key role to obtain the energy stability. In summary, the scheme (3.9)–(3.17) is a linear, decoupled scheme. At each time step, one only needs to solve a sequence of linear equations.

We now prove the unconditional energy stability as follows.

THEOREM 3.1. *Assuming* $S\geq\frac{1}{2}\lambda L$ *and* $\chi(\Phi)\leq\chi_0$, *then the solutions of the scheme* (3.9)–(3.17) *satisfy the following energy law:*

$$d_tE(\Phi^n,\boldsymbol{u}^n,\boldsymbol{h}^n,\boldsymbol{m}^n,p^n)+G^n\leq\frac{\mu}{\tau}\|\boldsymbol{h}_a^n\|^2+\tau\mu\|d_t\boldsymbol{h}_a^n\|^2, \tag{3.19}$$

where

$$\begin{aligned}E(\Phi^n,\boldsymbol{u}^n,\boldsymbol{h}^n,\boldsymbol{m}^n,p^n)=\lambda\Big(\frac{\epsilon}{2}\|\nabla\Phi^n\|^2+(F(\Phi^n),1)\Big)+\frac{1}{2}\|\boldsymbol{u}^n\|^2\\+\frac{\mu}{2}\|\boldsymbol{h}^n\|^2+\frac{\mu}{2\chi_0}\|\boldsymbol{m}^n\|^2+\frac{\delta t^2}{2}\|\nabla p^n\|^2,\end{aligned} \tag{3.20}$$

$$G^n = M\|\nabla W^n\|^2 + \|\sqrt{\nu(\Phi^n)}D(\tilde{\boldsymbol{u}}^n)\|^2 + \frac{\mu}{2\tau}\|\boldsymbol{h}^n\|^2 + \mu\beta\|\boldsymbol{m}^{n-1}\times\tilde{\boldsymbol{h}}^n\|^2 + \frac{3\mu}{4\chi_0\tau}\|\boldsymbol{m}^n\|^2. \tag{3.21}$$

Proof. By taking $\Lambda = W^n$ in (3.9), we obtain

$$(d_t\Phi^n, W^n) - (\boldsymbol{u}^{n-1}\Phi^{n-1}, \nabla W^n) + \frac{\delta t}{2}\|\Phi^{n-1}\nabla W^n\|^2 + M\|\nabla W^n\|^2 = 0. \tag{3.22}$$

By taking $X = d_t\Phi^n$ in (3.10), we obtain

$$\frac{\lambda\epsilon}{2\delta t}(\|\nabla\Phi^n\|^2 - \|\nabla\Phi^{n-1}\|^2 + \|\nabla\Phi^n - \nabla\Phi^{n-1}\|^2) + \frac{S}{\delta t}\|\Phi^n - \Phi^{n-1}\|^2 + \lambda(f(\Phi^{n-1}), d_t\Phi^n) = (W^n, d_t\Phi^n). \tag{3.23}$$

By taking $\boldsymbol{v} = \tilde{\boldsymbol{u}}^n$ in (3.11) and using (3.5), we get

$$\begin{aligned}
&\frac{1}{2\delta t}(\|\tilde{\boldsymbol{u}}^n\|^2 - \|\boldsymbol{u}^{n-1}\|^2 + \|\tilde{\boldsymbol{u}}^n - \boldsymbol{u}^{n-1}\|^2) + \|\sqrt{\nu(\Phi^n)}D(\tilde{\boldsymbol{u}}^n)\|^2 \\
&\quad - (p^{n-1}, \nabla\cdot\tilde{\boldsymbol{u}}^n) + (\Phi^{n-1}\nabla W^n, \tilde{\boldsymbol{u}}^n) \\
&\quad + \mu\delta t\|(\tilde{\boldsymbol{u}}^n\cdot\nabla)\boldsymbol{m}^{n-1}\|^2 + 2\mu\delta t\|(\nabla\cdot\tilde{\boldsymbol{u}}^n)\boldsymbol{m}^{n-1}\|^2 + \frac{\mu}{2}\delta t\|\boldsymbol{m}^{n-1}\times\nabla\times\tilde{\boldsymbol{u}}^n\|^2 \\
&= \mu((\boldsymbol{m}^{n-1}\cdot\nabla)\tilde{\boldsymbol{h}}^{n-1}, \tilde{\boldsymbol{u}}^n) + \mu(\boldsymbol{m}^{n-1}\times\nabla\times\tilde{\boldsymbol{h}}^{n-1}, \tilde{\boldsymbol{u}}^n) \\
&\qquad + \frac{\mu}{2}(\boldsymbol{m}^{n-1}\times\tilde{\boldsymbol{h}}^{n-1}, \nabla\times\tilde{\boldsymbol{u}}^n),
\end{aligned} \tag{3.24}$$

where the term $b(\boldsymbol{u}^{n-1}, \tilde{\boldsymbol{u}}^n, \tilde{\boldsymbol{u}}^n)$ vanishes due to the skew-symmetry.

We rewrite (3.13) as the following equivalent form:

$$\boldsymbol{u}^n + \delta t\nabla p^n = \tilde{\boldsymbol{u}}^n + \delta t\nabla p^{n-1}.$$

By taking the L^2 inner product of the above equation with itself on both sides, using (3.18), and integrating by parts, we deduce

$$\frac{1}{2\delta t}(\|\boldsymbol{u}^n\|^2 - \|\tilde{\boldsymbol{u}}^n\|^2) + \frac{\delta t}{2}(\|\nabla p^n\|^2 - \|\nabla p^{n-1}\|^2) = -(\nabla\cdot\tilde{\boldsymbol{u}}^n, p^{n-1}). \tag{3.25}$$

By combining (3.24) and (3.25), we obtain

$$\begin{aligned}
&\frac{1}{2\delta t}(\|\boldsymbol{u}^n\|^2 - \|\boldsymbol{u}^{n-1}\|^2 + \|\tilde{\boldsymbol{u}}^n - \boldsymbol{u}^{n-1}\|^2) + \|\sqrt{\nu(\Phi^n)}D(\tilde{\boldsymbol{u}}^n)\|^2 \\
&\quad + \frac{\delta t}{2}(\|\nabla p^n\|^2 - \|\nabla p^{n-1}\|^2) + (\Phi^{n-1}\nabla W^n, \tilde{\boldsymbol{u}}^n) \\
&\quad + \mu\delta t\|(\tilde{\boldsymbol{u}}^n\cdot\nabla)\boldsymbol{m}^{n-1}\|^2 + 2\mu\delta t\|(\nabla\cdot\tilde{\boldsymbol{u}}^n)\boldsymbol{m}^{n-1}\|^2 + \frac{\mu}{2}\delta t\|\boldsymbol{m}^{n-1}\times\nabla\times\tilde{\boldsymbol{u}}^n\|^2 \\
&= \mu((\boldsymbol{m}^{n-1}\cdot\nabla)\tilde{\boldsymbol{h}}^{n-1}, \tilde{\boldsymbol{u}}^n) + \mu(\boldsymbol{m}^{n-1}\times\nabla\times\tilde{\boldsymbol{h}}^{n-1}, \tilde{\boldsymbol{u}}^n) \\
&\qquad + \frac{\mu}{2}(\boldsymbol{m}^{n-1}\times\tilde{\boldsymbol{h}}^{n-1}, \nabla\times\tilde{\boldsymbol{u}}^n).
\end{aligned} \tag{3.26}$$

By taking $\boldsymbol{n} = -\mu\tilde{\boldsymbol{h}}^n$ in (3.14), we obtain

$$\begin{aligned}(3.27)\qquad \frac{\mu}{\tau}\|\sqrt{\chi(\Phi^n)}\tilde{\boldsymbol{h}}^n\|^2 + \mu\beta\|\boldsymbol{m}^{n-1}\times\tilde{\boldsymbol{h}}^n\|^2 - \mu(d_t\tilde{\boldsymbol{m}}^n,\tilde{\boldsymbol{h}}^n) - \frac{\mu}{\tau}(\tilde{\boldsymbol{m}}^n,\tilde{\boldsymbol{h}}^n)\\ = \mu((\tilde{\boldsymbol{u}}^n\cdot\nabla)\boldsymbol{m}^{n-1},\tilde{\boldsymbol{h}}^n) + \mu((\nabla\cdot\tilde{\boldsymbol{u}}^n)\boldsymbol{m}^{n-1},\tilde{\boldsymbol{h}}^n)\\ - \frac{\mu}{2}(\nabla\times\tilde{\boldsymbol{u}}^n\times\boldsymbol{m}^{n-1},\tilde{\boldsymbol{h}}^n).\end{aligned}$$

By taking $\psi = \varphi^n$ and $\boldsymbol{Z} = \tilde{\boldsymbol{m}}^n$ in (3.15) and (3.16), respectively, we derive

$$\|\nabla\varphi^n\|^2 + (\tilde{\boldsymbol{m}}^n,\nabla\varphi^n) = (\boldsymbol{h}_a^n,\nabla\varphi^n),\quad (\tilde{\boldsymbol{h}}^n,\tilde{\boldsymbol{m}}^n) = (\nabla\varphi^n,\tilde{\boldsymbol{m}}^n),$$

which yields

$$(3.28)\qquad \frac{\mu}{\tau}\|\nabla\varphi^n\|^2 + \frac{\mu}{\tau}(\tilde{\boldsymbol{h}}^n,\tilde{\boldsymbol{m}}^n) = \frac{\mu}{\tau}(\boldsymbol{h}_a^n,\nabla\varphi^n).$$

By applying d_t to (3.15), we get

$$(\nabla d_t\varphi^n,\nabla\psi) + (d_t\tilde{\boldsymbol{m}}^n,\nabla\psi) = (d_t\boldsymbol{h}_a^n,\nabla\psi).$$

Letting $\psi = \varphi^n$ in above equation and $\boldsymbol{Z} = d_t\tilde{\boldsymbol{m}}^n$ in (3.16), we have

$$(3.29)\quad (\nabla d_t\varphi^n,\nabla\varphi^n) + (d_t\tilde{\boldsymbol{m}}^n,\nabla\varphi^n) = (d_t\boldsymbol{h}_a^n,\nabla\varphi^n),\quad (\tilde{\boldsymbol{h}}^n,d_t\tilde{\boldsymbol{m}}^n) = (\nabla\varphi^n,d_t\tilde{\boldsymbol{m}}^n).$$

Note $\boldsymbol{h}^n = \nabla\varphi^n$; hence (3.29) becomes

$$(3.30)\qquad \frac{1}{2\delta t}(\|\boldsymbol{h}^n\|^2 - \|\boldsymbol{h}^{n-1}\|^2 + \|\boldsymbol{h}^n - \boldsymbol{h}^{n-1}\|^2) + (\tilde{\boldsymbol{h}}^n,d_t\tilde{\boldsymbol{m}}^n) = (d_t\boldsymbol{h}_a^n,\boldsymbol{h}^n).$$

By combining (3.27), (3.28), and (3.30), we derive

$$\begin{aligned}(3.31)\qquad &\frac{\mu}{2\delta t}(\|\boldsymbol{h}^n\|^2 - \|\boldsymbol{h}^{n-1}\|^2 + \|\boldsymbol{h}^n - \boldsymbol{h}^{n-1}\|^2)\\ &\quad + \frac{\mu}{\tau}\|\boldsymbol{h}^n\|^2 + \frac{\mu}{\tau}\|\sqrt{\chi(\Phi^n)}\tilde{\boldsymbol{h}}^n\|^2 + \mu\beta\|\boldsymbol{m}^{n-1}\times\tilde{\boldsymbol{h}}^n\|^2\\ &= \mu((\tilde{\boldsymbol{u}}^n\cdot\nabla)\boldsymbol{m}^{n-1},\tilde{\boldsymbol{h}}^n) + \mu((\nabla\cdot\tilde{\boldsymbol{u}}^n)\boldsymbol{m}^{n-1},\tilde{\boldsymbol{h}}^n) - \frac{\mu}{2}(\nabla\times\tilde{\boldsymbol{u}}^n\times\boldsymbol{m}^{n-1},\tilde{\boldsymbol{h}}^n)\\ &\quad + \frac{\mu}{\tau}(\boldsymbol{h}_a^n,\boldsymbol{h}^n) + \mu(d_t\boldsymbol{h}_a^n,\boldsymbol{h}^n).\end{aligned}$$

By combining (3.22), (3.23), (3.26), and (3.31), we derive

$$\begin{aligned}(3.32)\qquad &\frac{\lambda\epsilon}{2\delta t}(\|\nabla\Phi^n\|^2 - \|\nabla\Phi^{n-1}\|^2 + \|\nabla\Phi^n - \nabla\Phi^{n-1}\|^2) + \frac{S}{\delta t}\|\Phi^n - \Phi^{n-1}\|^2\\ &\quad + \frac{\delta t}{2}\|\Phi^{n-1}\nabla W^n\|^2 + M\|\nabla W^n\|^2\\ &\quad + \frac{1}{2\delta t}(\|\boldsymbol{u}^n\|^2 - \|\boldsymbol{u}^{n-1}\|^2 + \|\tilde{\boldsymbol{u}}^n - \boldsymbol{u}^{n-1}\|^2)\\ &\quad + \|\sqrt{\nu(\Phi^n)}D(\tilde{\boldsymbol{u}}^n)\|^2 + \frac{\delta t}{2}(\|\nabla p^n\|^2 - \|\nabla p^{n-1}\|^2)\\ &\quad + \mu\delta t\|(\tilde{\boldsymbol{u}}^n\cdot\nabla)\boldsymbol{m}^{n-1}\|^2 + 2\mu\delta t\|(\nabla\cdot\tilde{\boldsymbol{u}}^n)\boldsymbol{m}^{n-1}\|^2\end{aligned}$$

$$
\begin{aligned}
&+ \frac{\mu}{2}\delta t\|\boldsymbol{m}^{n-1}\times\nabla\times\tilde{\boldsymbol{u}}^n\|^2 + \frac{\mu}{2\delta t}(\|\boldsymbol{h}^n\|^2 - \|\boldsymbol{h}^{n-1}\|^2 + \|\boldsymbol{h}^n - \boldsymbol{h}^{n-1}\|^2)\\
&+ \frac{\mu}{\tau}\|\boldsymbol{h}^n\|^2 + \frac{\mu}{\tau}\|\sqrt{\chi(\Phi^n)}\tilde{\boldsymbol{h}}^n\|^2 + \mu\beta\|\boldsymbol{m}^{n-1}\times\tilde{\boldsymbol{h}}^n\|^2\\
&= (\boldsymbol{u}^{n-1}\Phi^{n-1}, \nabla W^n) - (\Phi^{n-1}\nabla W^n, \tilde{\boldsymbol{u}}^n) \qquad (:\text{ term I})\\
&+ \mu((\boldsymbol{m}^{n-1}\cdot\nabla)\tilde{\boldsymbol{h}}^{n-1}, \tilde{\boldsymbol{u}}^n) + \mu(\boldsymbol{m}^{n-1}\times\nabla\times\tilde{\boldsymbol{h}}^{n-1}, \tilde{\boldsymbol{u}}^n)\\
&+ \mu((\tilde{\boldsymbol{u}}^n\cdot\nabla)\boldsymbol{m}^{n-1}, \tilde{\boldsymbol{h}}^n) + \mu((\nabla\cdot\tilde{\boldsymbol{u}}^n)\boldsymbol{m}^{n-1}, \tilde{\boldsymbol{h}}^n) \qquad (:\text{ term II})\\
&+ \frac{\mu}{2}(\boldsymbol{m}^{n-1}\times\tilde{\boldsymbol{h}}^{n-1}, \nabla\times\tilde{\boldsymbol{u}}^n) - \frac{\mu}{2}(\nabla\times\tilde{\boldsymbol{u}}^n\times\boldsymbol{m}^{n-1}, \tilde{\boldsymbol{h}}^n) \qquad (:\text{ term III})\\
&- \lambda(f(\Phi^{n-1}), d_t\Phi^n) \qquad (:\text{ term IV})\\
&+ \frac{\mu}{\tau}(\boldsymbol{h}_a^n, \boldsymbol{h}^n) + \mu(d_t\boldsymbol{h}_a^n, \boldsymbol{h}^n). \qquad (:\text{ term V})
\end{aligned}
$$

We estimate terms I–V on the right-hand side of (3.32) as follows.

First, term I can be estimated as

$$
\begin{aligned}
\text{term I} &= (\boldsymbol{u}^{n-1}\Phi^{n-1}, \nabla W^n) - (\Phi^{n-1}\nabla W^n, \tilde{\boldsymbol{u}}^n)\\
&= (\Phi^{n-1}\nabla W^n, \boldsymbol{u}^{n-1} - \tilde{\boldsymbol{u}}^n)\\
&\le \|\Phi^{n-1}\nabla W^n\|\|\boldsymbol{u}^{n-1} - \tilde{\boldsymbol{u}}^n\|\\
&\le \frac{1}{2\delta t}\|\boldsymbol{u}^{n-1} - \tilde{\boldsymbol{u}}^n\|^2 + \frac{\delta t}{2}\|\Phi^{n-1}\nabla W^n\|^2.
\end{aligned} \tag{3.33}
$$

Second, by using Lemma 2.1 and integration by parts, term II can be estimated as

$$
\begin{aligned}
\text{term II} &= \mu((\boldsymbol{m}^{n-1}\cdot\nabla)\tilde{\boldsymbol{h}}^{n-1}, \tilde{\boldsymbol{u}}^n) + \mu(\boldsymbol{m}^{n-1}\times\nabla\times\tilde{\boldsymbol{h}}^{n-1}, \tilde{\boldsymbol{u}}^n) + \mu((\tilde{\boldsymbol{u}}^n\cdot\nabla)\boldsymbol{m}^{n-1}, \tilde{\boldsymbol{h}}^n)\\
&\qquad + \mu((\nabla\cdot\tilde{\boldsymbol{u}}^n)\boldsymbol{m}^{n-1}, \tilde{\boldsymbol{h}}^n)\\
&= \mu((\tilde{\boldsymbol{u}}^n\cdot\nabla)\tilde{\boldsymbol{h}}^{n-1}, \boldsymbol{m}^{n-1}) + \mu((\tilde{\boldsymbol{u}}^n\cdot\nabla)\boldsymbol{m}^{n-1}, \tilde{\boldsymbol{h}}^n) + \mu((\nabla\cdot\tilde{\boldsymbol{u}}^n)\boldsymbol{m}^{n-1}, \tilde{\boldsymbol{h}}^n)\\
&= \mu((\tilde{\boldsymbol{u}}^n\cdot\nabla)(\tilde{\boldsymbol{h}}^{n-1} - \tilde{\boldsymbol{h}}^n), \boldsymbol{m}^{n-1})\\
&= -\mu((\tilde{\boldsymbol{u}}^n\cdot\nabla)\boldsymbol{m}^{n-1}, \tilde{\boldsymbol{h}}^{n-1} - \tilde{\boldsymbol{h}}^n) - \mu((\nabla\cdot\tilde{\boldsymbol{u}}^n)\boldsymbol{m}^{n-1}, \tilde{\boldsymbol{h}}^{n-1} - \tilde{\boldsymbol{h}}^n)\\
&\le \mu\|(\tilde{\boldsymbol{u}}^n\cdot\nabla)\boldsymbol{m}^{n-1}\|\|\tilde{\boldsymbol{h}}^{n-1} - \tilde{\boldsymbol{h}}^n\| + \mu\|(\nabla\cdot\tilde{\boldsymbol{u}}^n)\boldsymbol{m}^{n-1}\|\|\tilde{\boldsymbol{h}}^{n-1} - \tilde{\boldsymbol{h}}^n\|\\
&\le \frac{\mu}{4\delta t}\|\tilde{\boldsymbol{h}}^{n-1} - \tilde{\boldsymbol{h}}^n\|^2 + \mu\delta t\|(\tilde{\boldsymbol{u}}^n\cdot\nabla)\boldsymbol{m}^{n-1}\|^2 + \frac{\mu}{8\delta t}\|\tilde{\boldsymbol{h}}^{n-1} - \tilde{\boldsymbol{h}}^n\|^2\\
&\qquad + 2\mu\delta t\|(\nabla\cdot\tilde{\boldsymbol{u}}^n)\boldsymbol{m}^{n-1}\|^2\\
&\le \frac{3\mu}{8\delta t}\|\boldsymbol{h}^{n-1} - \boldsymbol{h}^n\|^2 + \mu\delta t\|(\tilde{\boldsymbol{u}}^n\cdot\nabla)\boldsymbol{m}^{n-1}\|^2 + 2\mu\delta t\|(\nabla\cdot\tilde{\boldsymbol{u}}^n)\boldsymbol{m}^{n-1}\|^2,
\end{aligned} \tag{3.34}
$$

where we use the following identity:

$$
((\boldsymbol{u}\cdot\nabla)\boldsymbol{v}, \boldsymbol{w}) + ((\boldsymbol{u}\cdot\nabla)\boldsymbol{w}, \boldsymbol{v}) = -((\nabla\cdot\boldsymbol{u})\boldsymbol{v}, \boldsymbol{w}) \text{ if } \boldsymbol{u}\cdot n|_{\partial\Omega} = 0
$$

and the inequality $\|\tilde{\boldsymbol{h}}^n - \tilde{\boldsymbol{h}}^{n-1}\|^2 \le \|\boldsymbol{h}^n - \boldsymbol{h}^{n-1}\|^2$ which is derived by (3.16).

Third, we estimate term III as

$$\begin{aligned}\text{term III} &= \frac{\mu}{2}(\boldsymbol{m}^{n-1}\times\tilde{\boldsymbol{h}}^{n-1},\nabla\times\tilde{\boldsymbol{u}}^n)-\frac{\mu}{2}(\nabla\times\tilde{\boldsymbol{u}}^n\times\boldsymbol{m}^{n-1},\tilde{\boldsymbol{h}}^n)\\ &= \frac{\mu}{2}(\tilde{\boldsymbol{h}}^{n-1}-\tilde{\boldsymbol{h}}^n,\nabla\times\tilde{\boldsymbol{u}}^n\times\boldsymbol{m}^{n-1})\\ &\le \frac{\mu}{2}\|\tilde{\boldsymbol{h}}^{n-1}-\tilde{\boldsymbol{h}}^n\|\|\nabla\times\tilde{\boldsymbol{u}}^n\times\boldsymbol{m}^{n-1}\| \qquad (3.35)\\ &\le \frac{\mu}{8\delta t}\|\tilde{\boldsymbol{h}}^{n-1}-\tilde{\boldsymbol{h}}^n\|^2+\frac{\mu}{2}\delta t\|\boldsymbol{m}^{n-1}\times\nabla\times\tilde{\boldsymbol{u}}^n\|^2\\ &\le \frac{\mu}{8\delta t}\|\boldsymbol{h}^{n-1}-\boldsymbol{h}^n\|^2+\frac{\mu}{2}\delta t\|\boldsymbol{m}^{n-1}\times\nabla\times\tilde{\boldsymbol{u}}^n\|^2.\end{aligned}$$

Fourth, for term IV, by using the Taylor expansion, there exists ξ such that

$$F(\Phi^n)-F(\Phi^{n-1})=f(\Phi^{n-1})(\Phi^n-\Phi^{n-1})+\frac{1}{2}f'(\xi)(\Phi^n-\Phi^{n-1})^2.$$

Hence, from (2.3), we derive

$$\begin{aligned}(d_tF(\Phi^n),1) &= \frac{1}{\delta t}(F(\Phi^n)-F(\Phi^{n-1}),1)\\ &= (f(\Phi^{n-1}),d_t\Phi^n)+\frac{1}{2\delta t}(f'(\xi),(\Phi^n-\Phi^{n-1})^2)\\ &\le (f(\Phi^{n-1}),d_t\Phi^n)+\frac{L}{2\delta t}\|\Phi^n-\Phi^{n-1}\|^2,\end{aligned}$$

which implies

$$\text{term IV}=-\lambda(f(\Phi^{n-1}),d_t\Phi^n)\le-\lambda(d_tF(\Phi^n),1)+\frac{\lambda L}{2\delta t}\|\Phi^n-\Phi^{n-1}\|^2, \qquad (3.36)$$

$$\begin{aligned}\text{term V} &\le \frac{\mu}{\tau}\|\boldsymbol{h}_a^n\|\|\boldsymbol{h}^n\|+\mu\|d_t\boldsymbol{h}_a^n\|\|\boldsymbol{h}^n\| \qquad (3.37)\\ &\le \frac{\mu}{4\tau}\|\boldsymbol{h}^n\|^2+\frac{\mu}{\tau}\|\boldsymbol{h}_a^n\|^2+\frac{\mu}{4\tau}\|\boldsymbol{h}^n\|^2+\tau\mu\|d_t\boldsymbol{h}_a^n\|^2.\end{aligned}$$

By combining (3.32)–(3.37), we obtain

$$\begin{aligned}&\frac{\lambda\epsilon}{2\delta t}(\|\nabla\Phi^n\|^2-\|\nabla\Phi^{n-1}\|^2+\|\nabla\Phi^n-\nabla\Phi^{n-1}\|^2)\\ &\quad+\lambda(d_tF(\Phi^n),1)+\frac{1}{\delta t}\left(S-\frac{\lambda L}{2}\right)\|\Phi^n-\Phi^{n-1}\|^2+M\|\nabla W^n\|^2\\ &\quad+\frac{1}{2\delta t}(\|\boldsymbol{u}^n\|^2-\|\boldsymbol{u}^{n-1}\|^2)+\|\sqrt{\nu(\Phi^n)}D(\tilde{\boldsymbol{u}}^n)\|^2 \qquad (3.38)\\ &\quad+\frac{\delta t}{2}(\|\nabla p^n\|^2-\|\nabla p^{n-1}\|^2)+\frac{\mu}{2\delta t}(\|\boldsymbol{h}^n\|^2-\|\boldsymbol{h}^{n-1}\|^2)\\ &\quad+\frac{\mu}{2\tau}\|\boldsymbol{h}^n\|^2+\frac{\mu}{\tau}\|\sqrt{\chi(\Phi^n)}\tilde{\boldsymbol{h}}^n\|^2+\mu\beta\|\boldsymbol{m}^{n-1}\times\tilde{\boldsymbol{h}}^n\|^2\\ &\le \frac{\mu}{\tau}\|\boldsymbol{h}_a^n\|^2+\tau\mu\|d_t\boldsymbol{h}_a^n\|^2.\end{aligned}$$

By taking $\boldsymbol{n}=\frac{\mu}{\chi_0}\boldsymbol{m}^n$ in (3.17), we derive

$$\frac{\mu}{2\chi_0\delta t}(\|\boldsymbol{m}^n\|^2-\|\boldsymbol{m}^{n-1}\|^2+\|\boldsymbol{m}^n-\boldsymbol{m}^{n-1}\|^2)+\frac{\mu}{\tau\chi_0}\|\boldsymbol{m}^n\|^2=\frac{\mu}{\tau\chi_0}(\chi(\Phi^n)\tilde{\boldsymbol{h}}^n,\boldsymbol{m}^n). \qquad (3.39)$$

We estimate the term on the right-hand side as

$$\begin{aligned}\frac{\mu}{\tau\chi_0}(\chi(\Phi^n)\tilde{\boldsymbol{h}}^n,\boldsymbol{m}^n) &\le \frac{\mu}{\tau\chi_0}\|\sqrt{\chi(\Phi^n)}\tilde{\boldsymbol{h}}^n\|\|\sqrt{\chi(\Phi^n)}\boldsymbol{m}^n\|\\ &\le \frac{\mu}{\tau}\|\sqrt{\chi(\Phi^n)}\tilde{\boldsymbol{h}}^n\|^2+\frac{\mu}{4\tau\chi_0^2}\|\sqrt{\chi(\Phi^n)}\boldsymbol{m}^n\|^2\\ &\le \frac{\mu}{\tau}\|\sqrt{\chi(\Phi^n)}\tilde{\boldsymbol{h}}^n\|^2+\frac{\mu}{4\tau\chi_0}\|\boldsymbol{m}^n\|^2.\end{aligned}\tag{3.40}$$

Finally, by combining (3.38), (3.39), and (3.40), we obtain

$$\begin{aligned}&\frac{\lambda\epsilon}{2\delta t}(\|\nabla\Phi^n\|^2-\|\nabla\Phi^{n-1}\|^2+\|\nabla\Phi^n-\nabla\Phi^{n-1}\|^2)+\lambda(d_tF(\Phi^n),1)+M\|\nabla W^n\|^2\\ &\quad+\frac{1}{2\delta t}(\|\boldsymbol{u}^n\|^2-\|\boldsymbol{u}^{n-1}\|^2)+\|\sqrt{\nu(\Phi^n)}D(\tilde{\boldsymbol{u}}^n)\|^2\\ &\quad+\frac{\delta t}{2}(\|\nabla p^n\|^2-\|\nabla p^{n-1}\|^2)+\frac{\mu}{2\delta t}(\|\boldsymbol{h}^n\|^2-\|\boldsymbol{h}^{n-1}\|^2)+\frac{\mu}{2\tau}\|\boldsymbol{h}^n\|^2\\ &\quad+\mu\beta\|\boldsymbol{m}^{n-1}\times\tilde{\boldsymbol{h}}^n\|^2+\frac{\mu}{2\chi_0\delta t}(\|\boldsymbol{m}^n\|^2-\|\boldsymbol{m}^{n-1}\|^2+\|\boldsymbol{m}^n-\boldsymbol{m}^{n-1}\|^2)\\ &\quad+\frac{3\mu}{4\tau\chi_0}\|\boldsymbol{m}^n\|^2+\frac{1}{\delta t}\left(S-\frac{\lambda L}{2}\right)\|\Phi^n-\Phi^{n-1}\|^2\le\frac{\mu}{\tau}\|\boldsymbol{h}_a^n\|^2+\tau\mu\|d_t\boldsymbol{h}_a^n\|^2.\end{aligned}\tag{3.41}$$

After dropping several positive terms on the left-hand side, we obtain (3.19). ∎

Remark 3.6. It is worth noting that $\boldsymbol{h}_a$ is a given external magnetic field acting as a source term. Since it may change over time (cf. the numerical example in section 4.3), the symbol "$\boldsymbol{h}_a^n$" used in the numerical scheme only means that its value may change with time, but it does not mean that it needs to computed inside the scheme. Moreover, after multiplying δt on the both sides of (3.19) and summing up from $n=1$ to K, we can obtain the energy stability for $E(\Phi^K,\boldsymbol{u}^K,\boldsymbol{h}^K,\boldsymbol{m}^K,p^K)$ at $t=t^K$ that reads as

$$\begin{aligned}E(\Phi^K,\boldsymbol{u}^K,\boldsymbol{h}^K,\boldsymbol{m}^K,p^K)+\delta t\sum_{n=1}^{K}G^n &\le E(\Phi^0,\boldsymbol{u}^0,\boldsymbol{h}^0,\boldsymbol{m}^0,p^0)\\ &\quad+\delta t\sum_{n=1}^{K}\left(\frac{\mu}{\tau}\|\boldsymbol{h}_a^n\|^2+\tau\mu\|d_t\boldsymbol{h}_a^n\|^2\right).\end{aligned}$$

4. Numerical tests. We now present series of numerical experiments to validate the theoretical results derived in the previous section and demonstrate the efficiency, energy stability, and accuracy of the proposed numerical scheme (3.9)–(3.17). In all numerical tests, we choose $L=\frac{1}{2\epsilon}$, thus the stabilizing constant is $S=\frac{\lambda}{4\epsilon}$. We only present two-dimensional simulations in this paper to verify our scheme. It is quite challenging to implement the three-dimensional simulations due to the high computational cost while the scheme developed in this paper is applicable in three dimensions.

4.1. Accuracy tests for temporal and spatial discretizations. We now test the convergence rates of the proposed scheme (3.9)–(3.17). Let $\Omega=[0,1]^2$; we choose forcing functions such that the exact solutions for the system (2.4)–(2.9) are

$$
(4.1)\quad \begin{cases} \Phi(t,\boldsymbol{x}) = 0.5\sin(t)\cos(\pi x)\cos(\pi y) + 0.5, \\ \boldsymbol{u}(t,\boldsymbol{x}) = (\sin(t)\sin(\pi x)\sin(\pi(y+0.5)), \sin(t)\cos(\pi x)\cos(\pi(y+0.5)))\,, \\ p(t,\boldsymbol{x}) = \sin(t)(2x-1)(2y-1), \\ \boldsymbol{m}(t,\boldsymbol{x}) = (\sin(t+y), \sin(t+x))\,, \\ \varphi(t,\boldsymbol{x}) = (x-0.5)y\sin(t). \end{cases}
$$

We set the model parameters as follows:

$$
\epsilon = M = 0.05, \quad \nu_f = 2.0, \quad \nu_w = 1.0, \quad \lambda = \mu = \tau = \beta = \chi_0 = 1.0.
$$

We set the finite element spaces (3.6) with $l_1 = 1, l_2 = l_3 = 2$. In this way, the following optimal convergence error estimates are expected:

$$
(4.2)\quad \begin{aligned} &\|e_\Phi^n\|_{L^2} \lesssim \delta t + h^2,\ \|e_\Phi^n\|_{H^1} \lesssim \delta t + h,\ \|e_{\boldsymbol{u}}^n\|_{L^2} \lesssim \delta t + h^3, \\ &\|e_{\boldsymbol{u}}^n\|_{H^1} + \|e_p^n\|_{L^2} \lesssim \delta t + h^2,\ \|e_{\boldsymbol{h}}^n\|_{L^2} + \|e_{\boldsymbol{m}}^n\|_{L^2} \lesssim \delta t + h^2, \end{aligned}
$$

where $e_\psi^n = \psi(t_n) - \psi^n$ for any function ψ.

To verify the convergence orders of our scheme, we first set $\delta t = h$ and refine the spatial grid size with $h = 2^{-i}$, $i = 3$, 4, 5, 6, 7, and 8. According to (4.2), the convergent orders are expected to be

$$
\begin{aligned} &\|e_\Phi^n\|_{L^2} \lesssim \delta t + h^2 \lesssim h,\ \|e_\Phi^n\|_{H^1} \lesssim \delta t + h \lesssim h, \|e_{\boldsymbol{u}}^n\|_{L^2} \lesssim \delta t + h^3 \lesssim h, \\ &\|e_{\boldsymbol{u}}^n\|_{H^1} + \|e_p^n\|_{L^2} \lesssim \delta t + h^2 \lesssim h,\ \|e_{\boldsymbol{h}}^n\|_{L^2} + \|e_{\boldsymbol{m}}^n\|_{L^2} \lesssim \delta t + h^2 \lesssim h. \end{aligned}
$$

In Figure 4.1, we plot the computed errors at $t = 0.5$ with various grid sizes h, where we observe that all above error functions attain almost perfect first-order accuracy, which confirm the above predicted convergence rates.

Second, we set $\delta t = h^2$ and refine the meshes with $h = 2^{-i}$, $i = 3$, 4, 5, 6, and 7. Hence the convergent orders are expected to be

$$
\begin{aligned} &\|e_\Phi^n\|_{L^2} \lesssim \delta t + h^2 \lesssim h^2, \|e_{\boldsymbol{u}}^n\|_{L^2} \lesssim \delta t + h^3 \lesssim h^2, \\ &\|e_{\boldsymbol{u}}^n\|_{H^1} + \|e_p^n\|_{L^2} \lesssim \delta t + h^2 \lesssim h^2, \|e_{\boldsymbol{h}}^n\|_{L^2} + \|e_{\boldsymbol{m}}^n\|_{L^2} \lesssim \delta t + h^2 \lesssim h^2. \end{aligned}
$$

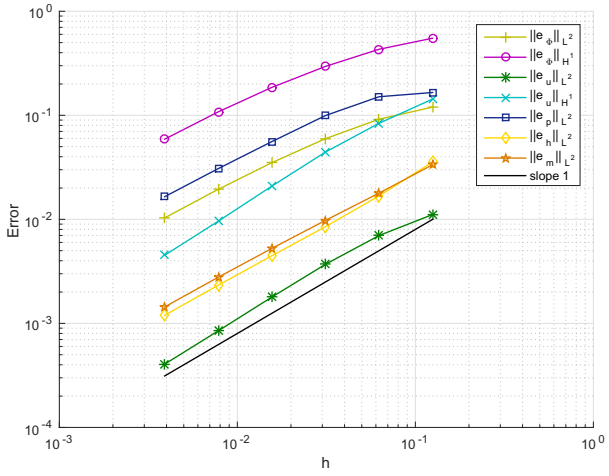

FIG. 4.1. *Convergent rates of the error functions of* $\|e_\Phi\|_{L^2}$, $\|e_\Phi\|_{H^1}$, $\|e_{\boldsymbol{u}}\|_{L^2}$, $\|e_{\boldsymbol{u}}\|_{H^1}$, $\|e_p\|_{L^2}$, $\|e_{\boldsymbol{h}}\|_{L^2}(\|\nabla e_\varphi\|_{L^2})$, *and* $\|e_{\boldsymbol{m}}\|_{L^2}$ *with* $\delta t = h$ *at* $t = 0.5$.

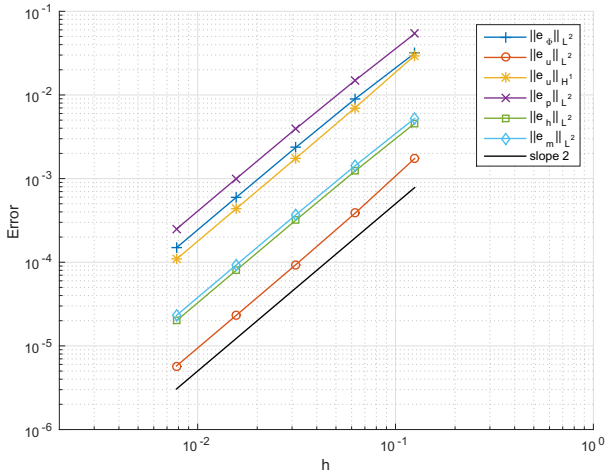

FIG. 4.2. *Convergent rates of the error functions of* $\|e_\Phi\|_{L^2}$, $\|e_{\boldsymbol{u}}\|_{L^2}$, $\|e_{\boldsymbol{u}}\|_{H^1}$, $\|e_p\|_{L^2}$, $\|e_{\boldsymbol{h}}\|_{L^2}(\|\nabla e_\varphi\|_{L^2})$, *and* $\|e_{\boldsymbol{m}}\|_{L^2}$ *with* $\delta t = h^2$ *at* $t = 0.5$.

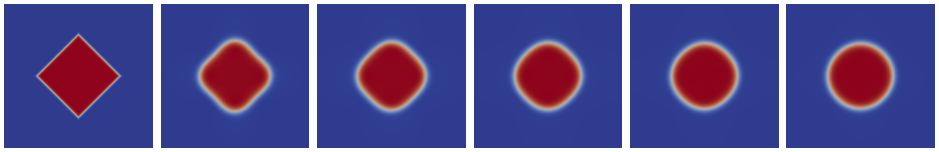

FIG. 4.3. *Snapshots of the phase field* Φ *are taken at* $t = 0$, 1, 2, 3, 4, *and* 5 *by using the time step* $\delta t = 1\text{e}{-3}$ *and grid size* $h = \frac{1}{64}$.

In Figure 4.2, we plot the computed errors at $t = 0.5$ with various grid sizes h. The convergent rates of all variables present the almost perfect second-order accuracy which is consistent with the above expected convergence orders.

4.2. Stability tests. In this subsection, we show the developed scheme (3.9)–(3.17) is unconditionally energy stable with various time steps. We set the computational domain $\Omega = [0, 2\pi]^2$ and use the same model parameters as the previous section. We set the finite element spaces (3.6) with $l_1 = 1, l_2 = l_3 = 2$. We impose the initial conditions and applied magnetic field as

$$\Phi_0 = 0.5 - 0.5 \tanh\left(\frac{|x - x_0| + |y - y_0| - r}{1.2\epsilon}\right),$$
$$\boldsymbol{u}_0 = (0, 0), \quad \boldsymbol{m}_0 = (0, 0), \quad \boldsymbol{h}_a = (0, 0),$$

where $(x_0, y_0, r) = (\pi, \pi, 1.75)$.

In Figure 4.3, we plot the snapshots of the phase field variable Φ at various times by using the time step size $\delta t = 1\text{e}{-3}$ and mesh size $h = \frac{1}{64}$. We observe that a square at the $t = 0$ gradually evolves into a circle under the effects of surface tensions. In Figure 4.4, we plot the total free energy (3.20) until $t = 5$ by using various time steps and fixing $h = \frac{1}{64}$. For all tested time steps, the obtained energy curves show the monotonic decays that confirms that the developed scheme is unconditionally stable.

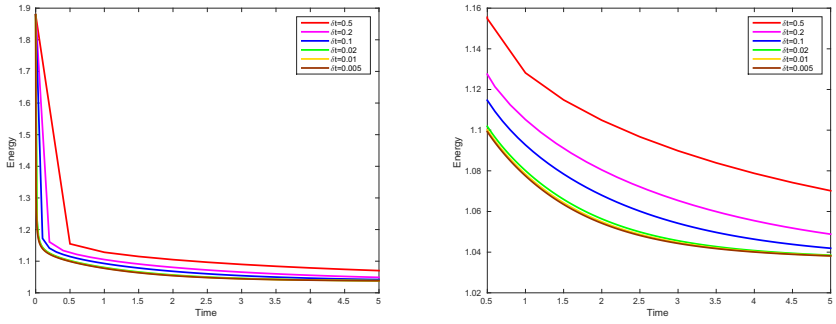

(a) Energy evolution. (b) A close-up view.

FIG. 4.4. (a) *Time evolution of the total free energy by using six different time step sizes where* $\delta t = 0.5,\ 0.2,\ 0.1,\ 0.02,\ 0.01,$ *and* 0.005. (b) *A close-up view of the free energy evolution for* $t \in [0.5, 5]$.

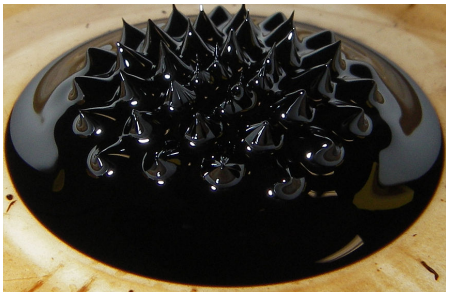

FIG. 4.5. *A ferrofluid in a magnetic field (from Wikipedia).*

4.3. Rosensweig instability under uniformly applied magnetic field. We now simulate a benchmark simulation, the so-called *Rosensweig instability* (also called normal-field instability; cf. [1, 15, 17, 18, 21, 33]) to validate the developed model (2.4)–(2.9) and show the robustness of our scheme (3.9)–(3.17). Figure 4.5 presents the spike shape of a ferrofluid drop that is situated on the substrate caused by a neodymium magnet beneath the dish (from Wikipedia).

We consider a mixture of ferrofluid and nonferrofluid with different viscosities and almost matching densities. We supplement the gravity force as a forcing term $\boldsymbol{f}_g$ on the right-hand side of (2.6), where the Boussinesq approximation is used, i.e.,

$$\boldsymbol{f}_g = \left(1 + \frac{r}{1 + e^{\frac{1-2\Phi}{\epsilon}}}\right)\boldsymbol{g},$$

where r is a positive constant depending on fluid density and $|\boldsymbol{g}|$ stands for the magnitude of gravity. A linear combination of dipoles is used as the applied magnetizing field $\boldsymbol{h}_a$ that reads as

$$\boldsymbol{h}_a = \sum_s \alpha_s \nabla\phi_s(\boldsymbol{x}), \quad \phi_s(\boldsymbol{x}) = \frac{\boldsymbol{d}\cdot(\boldsymbol{x}_s - \boldsymbol{x})}{|\boldsymbol{x}_s - \boldsymbol{x}|^2},$$

where $|\boldsymbol{d}| = 1$ indicates the direction of the dipole and $\boldsymbol{x}_s$ is the dipole's position. It is easy to verify that $\nabla\phi_s$ defines a harmonic field (i.e., $\nabla\times\nabla\phi_s = 0$, $\mathrm{div}\nabla\phi_s = 0$).

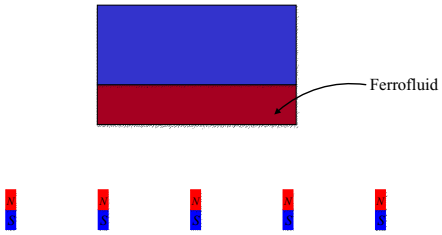

FIG. 4.6. *The sketch of the setup of Rosensweig instability under uniformly applied magnetic field.*

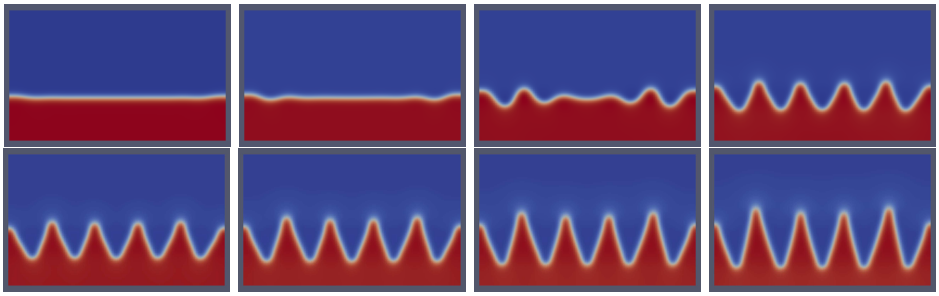

FIG. 4.7. *Snapshots of the phase variable* Φ *at* $t = 0.7$, 0.8, 0.9, 1, 1.1, 1.2, 1.3, *and* 1.4 *with the uniformly applied magnetic field.*

We set the computational domain: $\Omega = [0,1] \times [0,0.6]$ and the initial condition as

$$\Phi(t=0) = \begin{cases} 1 & y \le 0.2, \\ 0 & y > 0.2. \end{cases} \tag{4.3}$$

The model parameters are set as

$$\begin{cases} \epsilon = 5\text{e}{-3}, M = 2\text{e}{-4}, \nu_f = 2, \nu_w = 1, \mu = 1, \tau = 1\text{e}{-4}, \\ \beta = 1, \chi_0 = 0.5, \lambda = 1, r = 0.1, h = 1\text{e}{-2}, \delta t = 1\text{e}{-3}, \boldsymbol{g} = (0, -6\text{e}4). \end{cases} \tag{4.4}$$

We set the finite element spaces (3.6) with $l_1 = l_2 = l_3 = 2$.

To generate an approximate uniform applied magnetic field, we place five dipoles with far distance from the computational domain. The positions $\boldsymbol{x}_s$ of dipoles are $(-0.5, -15)$, $(0, -15)$, $(0.5, -15)$, $(1, -15)$, and $(1.5, -15)$, and the direction $\boldsymbol{d}$ of the five dipoles are all $(0, 1)$. The intensity α_s is the same for the five dipoles but increases linearly in time, starting from $\alpha_s = 0$ at time $t = 0$ to maximum value $\alpha_s = 8000$ at time $t = 1.6$, and from $t = 1.6$ the intensity is kept constant. Figure 4.6 demonstrates how the ferrofluid and dipoles are set up.

In Figure 4.7, we plot the snapshots of the phase variable Φ at various times. We observe that six spikes appear and the directions of "sawtooth" are aligned with the applied magnetic field (pointing upward). In Figure 4.8, we plot the velocity streamlines where pairs of vortexes are formed with the time. In Figure 4.9, we plot the magnetization field $\boldsymbol{m}$ and the effective magnetizing field $\boldsymbol{h}$ at $t = 1.4$. In the non-ferromagnetic phase, magnetization field $\boldsymbol{m}$ is almost zero, and the effective magnetic field $\boldsymbol{h}$ is equal to applied magnetic field $\boldsymbol{h}_a$. These simulations are qualitatively consistent with the experimental results shown in Figure 4.5 and the numerical results presented in [33].

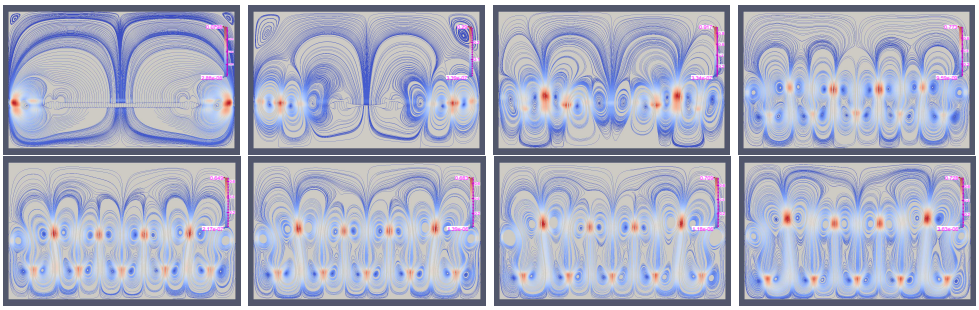

FIG. 4.8. *Snapshots of the velocity streamlines at* $t = 0.7$, 0.8, 0.9, 1, 1.1, 1.2, 1.3, *and* 1.4 *with the uniformly applied magnetic field.*

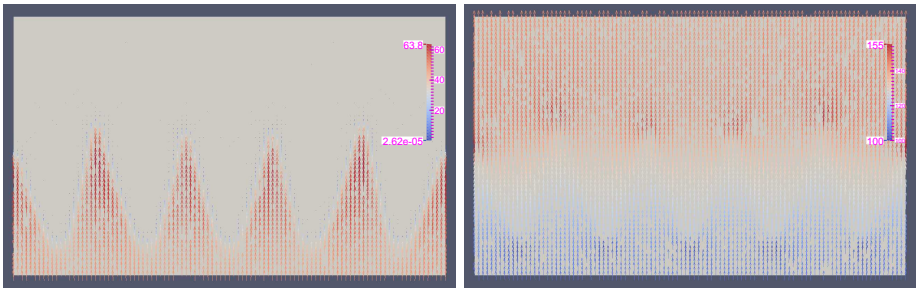

(a) The magnetization field $\boldsymbol{m}$. (b) The effective magnetizing field $\boldsymbol{h}$.

FIG. 4.9. *Snapshots of the magnetization field* $\boldsymbol{m}$ *and effective magnetizing field* $\boldsymbol{h}$ *at* $t = 1.4$ *with the uniformly applied magnetic field.*

4.4. Rosensweig instability under nonuniformly applied magnetic field. We further simulate the *Rosensweig instability* under a nonuniformly applied magnetic field. We set the initial condition of Φ as

$$\Phi(t=0) = \begin{cases} 1, & y \le 0.1, \\ 0, & y > 0.1. \end{cases} \tag{4.5}$$

All model parameters are still (4.4) but with $\chi_0 = 0.9$, $h = \frac{1}{120}$, and $\delta t = 2\text{e}{-4}$.

The applied magnetic field $\boldsymbol{h}_a = \sum_s \alpha_s \nabla \phi_s$ is generated by 42 dipoles. The dipoles are placed in three rows, at $y = -0.5$, $y = -0.75$, and $y = -1.0$, and the 14 pointing upwards ($\boldsymbol{d} = (0, 1)$) dipoles in each row are equidistributed in the x direction. The intention of this setup of the dipoles is to create a crude approximation of a bar magnet of 0.4 units width and 0.5 units height. The intensity α_s is the same for every dipole but increases linearly in time with a slope of 1.2 ($\alpha_s = 0$ at $t = 0$). The sketch of setup is shown in Figure 4.10; see also [33].

In Figure 4.11, we plot the snapshots of the phase variable Φ at various times. In contrast to the uniformly applied magnetic field case shown in Figure 4.7, the spikes exhibit a radiative pattern. The velocity streamlines, shown in Figure 4.12, present more complex irregular distributions. In Figure 4.13, we plot the magnetization field $\boldsymbol{m}$ and the effective magnetizing field $\boldsymbol{h}$ at $t = 3$.

4.5. Deformation of a ferrofluid droplet under uniformly applied magnetic field. In this subsection, we simulate the deformation of a ferrofluid droplet

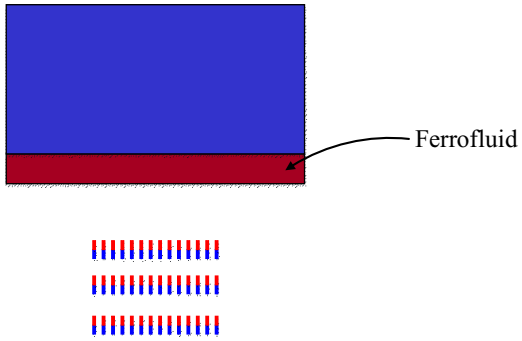

FIG. 4.10. *The sketch of the setup of Rosensweig instability under the nonuniformly applied magnetic field.*

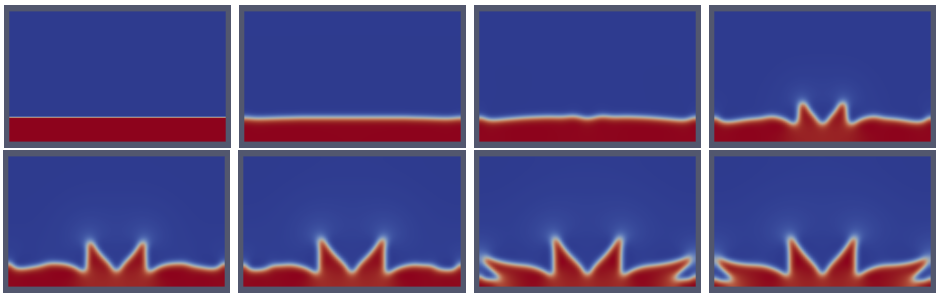

FIG. 4.11. *Snapshots of the phase variable* Φ *at* $t = 0$, 0.5, 1, 1.5, 2, 2.5, 3, *and* 3.5 *with the nonuniformly applied magnetic field.*

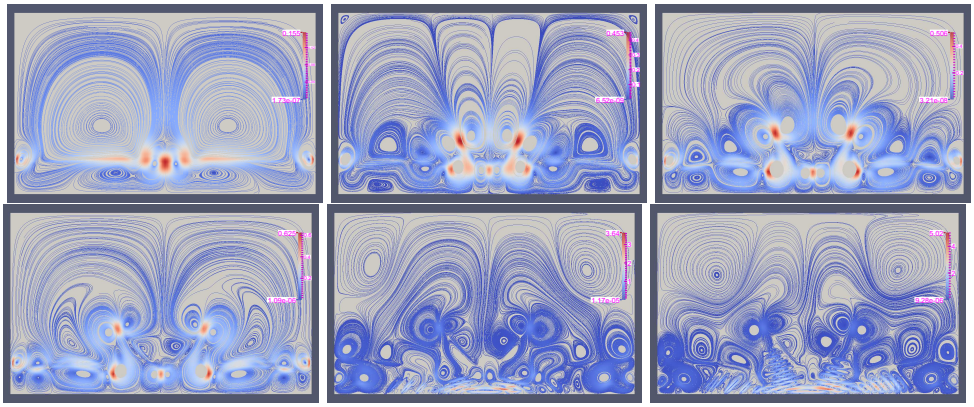

FIG. 4.12. *Snapshots of velocity streamlines at* $t = 1$, 1.5, 2, 2.5, 3, *and* 3.5 *with the nonuniformly applied magnetic field.*

suspended in a viscous medium under the uniformly applied uniform magnetic field. The equilibrium shape of the ferrofluid droplet is determined by the ratio of magnetic effect to surface tension effect, which can be characterized by the magnetic bond number [2]:

$$Bo_m = \frac{\mu H_0^2}{\lambda \kappa_0},$$

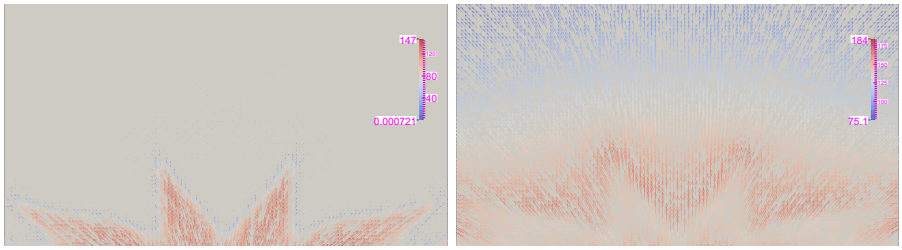

(a) The magnetization field $\boldsymbol{m}$. (b) The effective magnetizing field $\boldsymbol{h}$.

FIG. 4.13. *Snapshots of the magnetization field* $\boldsymbol{m}$ *and effective magnetizing field* $\boldsymbol{h}$ *at* $t = 3$ *with the nonuniformly applied magnetic field.*

where H_0 is the external applied magnetic strength and κ_0 is the curvature of the initial undeformed droplet with radius R_0 and $\kappa_0 = 2/R_0$. When Bo_m increases, the magnetic effect dominates the surface tension such that the interface tends to be parallel to the magnetic field, and thus the ferrodroplet will deform and be elongated gradually.

An analytic expression associated with the ratio $= b/a$ of deformed ferrodroplet and the magnetic bond number is derived in [2]:

$$Bo_m = \left[\frac{1}{\chi_0} + k\right]^2 \left(\frac{b}{a}\right)^{\frac{1}{3}} \left(2\frac{b}{a} - \left(\frac{b}{a}\right)^{-2} - 1\right), \tag{4.6}$$

where $2a$ and $2b$ are the minor axis and the major axis of deformed droplet, respectively. The parameter k is called the demagnetizing factor:

$$k = \left(\frac{1 - E^2}{2E^3}\right)\left(\ln\frac{1+E}{1-E} - 2E\right),$$

where $E = \sqrt{1 - a^2/b^2}$ is called eccentricity.

We set the computational domain: $\Omega = [0, 1]^2$ and the initial condition as

$$\Phi(t = 0) = \begin{cases} 1, & \sqrt{(x - 0.5)^2 + (y - 0.5)^2} \le 0.1, \\ 0 & \text{otherwise.} \end{cases} \tag{4.7}$$

The model parameters are set as

$$\begin{cases} \epsilon = 2\text{e}{-3}, M = 2\text{e}{-4}, \nu_f = \nu_w = 1, \mu = 0.1, \tau = 1\text{e}{-4}, \\ \beta = 1, \chi_0 = 2, \lambda = 1, h = \dfrac{1}{128}, \delta t = 1\text{e}{-3}. \end{cases} \tag{4.8}$$

To generate an uniform applied magnetic field, we place five dipoles with a far distance where the positions $\boldsymbol{x}_s$ of dipoles are $(-0.5, -15)$, $(0, -15)$, $(0.5, -15)$, $(1, -15)$, and $(1.5, -15)$. The directions $\boldsymbol{d}$ of the five dipoles are $(0, 1)$, and the intensity α_s is the same for the five dipoles but increases linearly in time with a slope of 1000, starting from $\alpha_s = 0$ at time $t = 0$.

In Figures 4.14–4.15, we plot the snapshots of the ferrodroplet at $t = 0$, 0.25, 0.5, 0.75, 1, 1.25, and 1.5. We observe the ferrodroplet is elongated with time and most of the interface tends to be parallel to the direction of the applied magnetic field $(0, 1)$. We plot the quantitative comparison between the analytical solution (4.6) and the computed results in Figure 4.16, where the numerical results agree with the analytical results well.

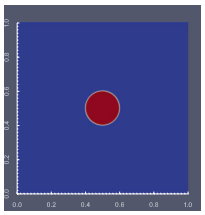

FIG. 4.14. *Snapshots of the phase field variable* Φ *at* $t = 0$.

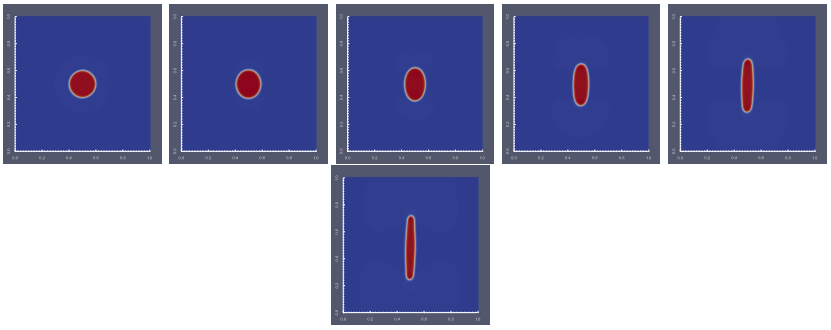

FIG. 4.15. *Drop deformation of a ferrofluid droplet under uniformly applied magnetic field. Snapshots of the phase field variable* Φ *at* $t = 0.25$, 0.5, 0.75, 1, 1.25, *and* 1.5.

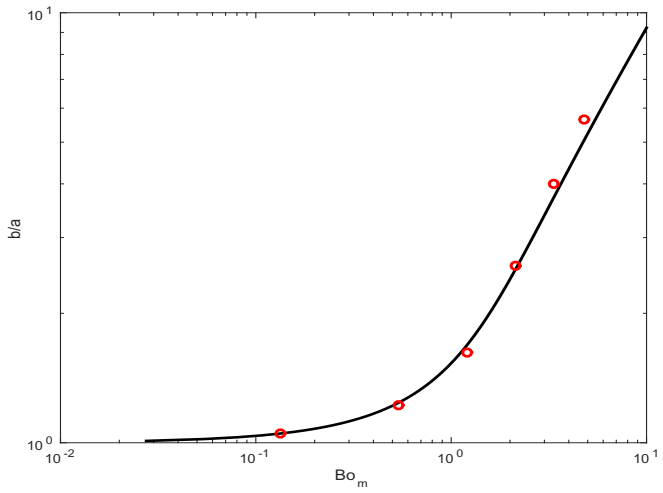

FIG. 4.16. *Comparison between the numerical results and analytical results. Solid line represents the analytical solution* (4.6)*; small red circles stand for numerical results.*

5. Conclusions. We consider the full discretization of a highly coupled nonlinear phase field model for the two-phase ferrofluids system. By combining several approaches which have proved to be effective for dealing with different difficulties of the nonlinear system, we construct a linear, decoupled, fully discrete scheme to solve the highly nonlinear and coupled multiphysics system efficiently. The scheme is provably unconditionally energy stable and leads to a series of decoupled linear equations

to solve at each time step. To the best of our knowledge, the scheme is the first decoupled, linear, unconditionally energy stable scheme for the phase-field model of two-phase ferrofluid flows.

REFERENCES

[1] B. Abou, J.-E. Wesfreid, and S. Roux, *The normal field instability in ferrofluids: Hexagon-square transition mechanism and wavenumber selection*, J. Fluid Mech., 416 (2000), pp. 217–237.

[2] S. Afkhami, A. J. Tyler, Y. Renardy, M. Renardy, T. G. St. Pierre, R. C. Woodward, and J. S. Riffle, *Deformation of a hydrophobic ferrofluid droplet suspended in a viscous medium under uniform magnetic fields*, J. Fluid Mech., 663 (2010), pp. 358–384.

[3] Y. Amirat and K. Hamdache, *Strong solutions to the equations of a ferrofluid flow model*, J. Math. Anal. Appl., 353 (2009), pp. 271–294.

[4] Y. Amirat, K. Hamdache, and F. Murat, *Global weak solutions to equations of motion for magnetic fluids*, J. Math. Fluid Mech., 10 (2008), pp. 326–351.

[5] F. Bai, D. Han, X.-M. He, and X. Yang, *Deformation and coalescence of ferrodroplets in Rosensweig model using the phase field and modified level set approaches under uniform magnetic fields*, Commun. Nonlinear Sci. Numer. Simul., 85 (2020), 105213.

[6] F. Bai, X.-M. He, R. Zhou, X. Yang, and C. Wang, *Three dimensional phase-field investigation of droplet formation in microfluidic flow focusing devices with experimental validation*, Int. J. Multiph. Flow, 93 (2017), pp. 130–141.

[7] F. Boyer and S. Minjeaud, *Numerical schemes for a three component Cahn-Hilliard model*, ESAIM Math. Model. Numer. Anal., 45 (2011), pp. 697–738.

[8] J. Byrom and S. L. Biswal, *Magnetic field directed assembly of two-dimensional fractal colloidal aggregates*, Soft Matter, 9 (2013), pp. 9167–9173.

[9] J. Byrom, P. Han, M. Savory, and S. L. Biswal, *Directing assembly of DNA-coated colloids with magnetic fields to generate rigid, semiflexible, and flexible chains*, Langmuir, 30 (2014), pp. 9045–9052.

[10] A. Chaves and C. Rinaldi, *Interfacial stress balances in structured continua and free surface flows in ferrofluids*, Phys. Fluids, 26 (2014), 042101.

[11] C. Chen and X. Yang, *Efficient numerical scheme for a dendritic solidification phase field model with melt convection*, J. Comput. Phys., 388 (2019), pp. 41–62.

[12] C. Chen and X. Yang, *Fast, provably unconditionally energy stable, and second-order accurate algorithms for the anisotropic Cahn-Hilliard Model*, Comput. Methods Appl. Mech. Engrg., 351 (2019), pp. 35–59.

[13] K. Cheng, W. Feng, C. Wang, and S. M. Wise, *An energy stable fourth order finite difference scheme for the Cahn-Hilliard equation*, J. Comput. Appl. Math., 362 (2019), pp. 574–595.

[14] K. Cheng, Z. Qiao, and C. Wang, *A third order exponential time differencing numerical scheme for no-slope-selection epitaxial thin film model with energy stability*, J. Sci. Comput., 81 (2019), pp. 154–185.

[15] M. D. Cowley and R. E. Rosensweig, *The interfacial stability of a ferromagnetic fluid*, J. Fluid Mech., 30 (1967), pp. 671–688.

[16] D. J. Eyre, *Unconditionally gradient stable time marching the Cahn–Hilliard equation*, in Computational and Mathematical Models of Microstructural Evolution (San Francisco, CA, 1998), Cambridge University Press, Cambridge, UK, 1998, pp. 39–46.

[17] R. Friedrichs and A. Engel, *Pattern and wave number selection in magnetic fluids*, Phys. Rev. E, 64 (2001), 021406, https://doi.org/10.1103/PhysRevE.64.021406.

[18] A. Gailitis, *Formation of the hexagonal pattern on the surface of a ferromagnetic fluid in an applied magnetic field*, J. Fluid Mech., 82 (1977), pp. 401–413.

[19] Y. Gao, X.-M. He, L. Mei, and X. Yang, *Decoupled, linear, and energy stable finite element method for the Cahn–Hilliard–Navier–Stokes–Darcy phase field model*, SIAM J. Sci. Comput., 40 (2018), pp. B110–B137.

[20] V. Girault and P. Raviart, *Finite Element Method for Navier-Stokes Equations: Theory and Algorithms*, Springer-Verlag, Berlin, 1987.

[21] C. Gollwitzer, G. Matthies, R. Richter, I. Rehberg, and L. Tobiska, *The surface topography of a magnetic fluid: A quantitative comparison between experiment and numerical simulation*, J. Fluid Mech., 571 (2007), pp. 455–474.

[22] H. Gomez and X. Nogueira, *An unconditionally energy-stable method for the phase field crystal equation*, Comput. Methods Appl. Mech. Engrg., 249-252 (2012), pp. 52–61.

[23] J. L. Guermond, P. Minev, and J. Shen, *An overview of projection methods for incompressible flows*, Comput. Methods Appl. Mech. Engrg., 195 (2006), pp. 6011–6045.
[24] J. L. Guermond and L. Quartapelle, *A projection FEM for variable density incompressible flows*, J. Comput. Phys., 165 (2000), pp. 167–188.
[25] J. L. Guermond and J. Shen, *On the error estimates of rotational pressure-correction projection methods.*, Math. Comp., 73 (2004), pp. 1719–1737.
[26] H. Hartshorne, C. J. Backhouse, and W. E. Lee, *Ferrofluid-based microchip pump and valve*, Sensor Actuat. B, 99 (2004), pp. 592–600.
[27] A. Hatch, A. E. Kamholz, G. Holman, P. Yager, and K. F. Bohringer, *A ferrofluidic magnetic micropump*, J. Microelectromech. Syst., 10 (2001), pp. 215–221.
[28] R. Li, Y. Gao, J. Chen, L. Zhang, X.-M. He, and Z. Chen, *Discontinuous finite volume element method for a coupled Navier-Stokes-Cahn-Hilliard phase field model*, Adv. Comput. Math., 46 (2020), 25.
[29] F. Lin, X.-M. He, and X. Wen, *Fast, unconditionally energy stable large time stepping method for a new Allen-Cahn type square phase-field crystal model*, Appl. Math. Lett., 92 (2019), pp. 248–255.
[30] L. Mao and H. Koser, *Ferrohydrodynamic pumping in spatially traveling sinusoidally time-varying magnetic fields*, J. Magn. Magn. Mater., 289 (2005), pp. 199–202.
[31] L. Mao and H. Koser, *Towards ferrofluidics for μ-TAS and lab on-a-chip applications*, Nanotechnology, 17 (2006), pp. S34–S47.
[32] O. T. Mefford, R. C. Woodward, J. D. Goff, T. P. Vadala, T. G. S. Pierre, J. P. Dailey, and J. S. Riffle, *Field-induced motion of ferrofluids through immiscible viscous media: Testbed for restorative treatment of retinal detachment*, J. Magn. Magn. Mater., 311 (2007), pp. 347–353.
[33] R. H. Nochetto, A. J. Salgado, and I. Tomas, *A diffuse interface model for two-phase ferrofluid flows*, Comput. Methods Appl. Mech. Engrg., 309 (2016), pp. 497–531.
[34] R. H. Nochetto, A. J. Salgado, and I. Tomas, *The equations of ferrohydrodynamics: Modeling and numerical methods*, Math. Models Methods Appl. Sci., 26 (2016), pp. 2393–2449.
[35] S. Odenbach, *Recent progress in magnetic fluid research*, J. Phys. Condensed Matter, 16 (2004), pp. R1135–R1150.
[36] S. Pal, A. Datta, S. Sen, A. Mukhopdhyay, K. Bandopadhyay, and R. Ganguly, *Characterization of a ferrofluid-based thermomagnetic pump for microfluidic applications*, J. Magn. Magn. Mater., 323 (2011), pp. 2701–2709.
[37] A. Prohl, *Projection and Quasi-Compressibility Methods for Solving the Incompressible Navier-Stokes Equations*, Adv. Numer. Math., Teubner, Stuttgart, 1997.
[38] K. Raj, B. Moskowitz, and R. Casciari, *Advances in ferrofluid technology*, J. Magn. Magn. Mater., 149 (1995), pp. 174–180.
[39] R. Rannacher, *On Chorin's projection method for the incompressible Navier-Stokes equations*, in The Navier-Stokes Equations II–Theory and Numerical Methods, J. G. Heywood, K. Masuda, R. Rautmann, and V. A. Solonnikov, eds., Springer, Berlin, 1991, pp. 167–183.
[40] C. Rinaldi and M. Zahn, *Effects of spin viscosity on ferrofluid duct flow profiles in alternating and rotating magnetic fields*, Phys. Fluids, 14 (2002), pp. 2847–2870.
[41] R. E. Rosensweig, *Ferrohydrodynamics*, Cambridge University Press, Cambridge, UK, 1985.
[42] R. E. Rosensweig, *Magnetic fluids*, Ann. Rev. Fluid Mech., 19 (1987), pp. 437–461.
[43] C. W. S. M. Wise and J. S. Lowengrub, *An energy-stable and convergent finite-difference scheme for the phase field crystal equation*, SIAM J. Numer. Anal., 47 (2009), pp. 2269–2288.
[44] J. Shen, *On error estimates of the projection methods for the Navier–Stokes equations: First-order schemes*, SIAM J. Numer. Anal., 29 (1992), pp. 57–77.
[45] J. Shen, *On error estimates of projection methods for the Navier-Stokes equations: Second-order schemes*, Math. Comp., 65 (1996), pp. 1039–1065.
[46] J. Shen, C. Wang, S. Wang, and X. Wang, *Second-order convex splitting schemes for gradient flows with Ehrlich–Schwoebel type energy: Application to thin film epitaxy*, SIAM J. Numer. Anal., 50 (2012), pp. 105–125.
[47] J. Shen and J. Xu, *Convergence and error analysis for the scalar auxiliary variable (SAV) schemes to gradient flows*, SIAM J. Numer. Anal., 56 (2018), pp. 2895–2912.
[48] J. Shen, J. Xu, and J. Yang, *The scalar auxiliary variable (SAV) approach for gradient flows*, J. Comput. Phys., 352 (2018), pp. 407–417.
[49] J. Shen and X. Yang, *Energy stable schemes for Cahn-Hilliard phase-field model of two-phase incompressible flows*, Chinese Ann. Math. Ser. B, 31 (2010), pp. 743–758.
[50] J. Shen and X. Yang, *Decoupled energy stable schemes for phase field models of two phase complex fluids*, SIAM J. Sci. Comput., 36 (2014), pp. B122–B145.

[51] J. Shen and X. Yang, *Decoupled, energy stable schemes for phase-field models of two-phase incompressible flows*, SIAM J. Num. Anal., 53 (2015), pp. 279–296.
[52] M. I. Shliomis, *Effective viscosity of magnetic suspensions*, Sov. Phys. Jetp, 34 (1972), pp. 1291–1294.
[53] M. I. Shliomis, *Ferrohydrodynamics: Retrospective and issues*, Lect. Notes Phys., 594 (2002), pp. 85–111.
[54] S. Venkatasubramanian and P. N. Kaloni, *Stability and uniqueness of magnetic fluid motions*, Proc. Math. Phys. Eng. Sci., 458 (2002), pp. 1189–1204.
[55] C. Wang and S. M. Wise, *An energy stable and convergent finite-difference scheme for the modified phase field crystal equation*, SIAM J. Numer. Anal., 49 (2011), pp. 945–969.
[56] C. Xu, C. Chen, X. Yang, and X.-M. He, *Numerical approximations for the hydrodynamics coupled binary surfactant phase field model: Second order, linear, unconditionally energy stable schemes*, Commun. Math. Sci., 17 (2019), pp. 835–858.
[57] J. Yang, S. Mao, X.-M. He, X. Yang, and Y. He, *A diffuse interface model and semi-implicit energy stable finite element method for two-phase magnetohydrodynamic flows*, Comput. Methods Appl. Mech. Eng., 356 (2019), pp. 435–464.
[58] X. Yang, *Linear, first and second order and unconditionally energy stable numerical schemes for the phase field model of homopolymer blends*, J. Comput. Phys., 327 (2016), pp. 294–316.
[59] X. Yang, *Efficient Linear, stabilized, second order time marching schemes for an anisotropic phase field dendritic crystal growth model*, Comput. Methods Appl. Mech. Engrg., 351 (2019), pp. 316–339.
[60] X. Yang, J. J. Feng, C. Liu, and J. Shen, *Numerical simulations of jet pinching-off and drop formation using an energetic variational phase-field method*, J. Comput. Phys., 218 (2006), pp. 417–428.
[61] X. Yang and D. Han, *Linearly first- and second-order, unconditionally energy stable schemes for the phase field crystal equation*, J. Comput. Phys., 330 (2017), pp. 1116–1134.
[62] X. Yang and H. Yu, *Efficient second order unconditionally stable schemes for a phase field moving contact line model using an invariant energy quadratization approach*, SIAM J. Sci. Comput., 40 (2018), pp. B889–B914.
[63] X. Yang, J. Zhao, and X.-M. He, *Linear, second order and unconditionally energy stable schemes for the viscous Cahn-Hilliard equation with hyperbolic relaxation using the invariant energy quadratization method*, J. Comput. Appl. Math., 343 (2018), pp. 80–97.
[64] X. Yang, J. Zhao, Q. Wang, and J. Shen, *Numerical approximations for a three components Cahn-Hilliard phase-field model based on the invariant energy quadratization method*, Math. Models Methods Appl. Sci., 27 (2017), pp. 1993–2030.
[65] B. B. Yellen, O. Hovorka, and G. Friedman, *Arranging matter by magnetic nanoparticle assemblers*, Proc. Natl. Acad. Sci. USA, 102 (2005), pp. 8860–8864.
[66] J. Zhao, X. Yang, J. Li, and Q. Wang, *Energy stable numerical schemes for a hydrodynamic model of nematic liquid crystals*, SIAM. J. Sci. Comput., 38 (2016), pp. A3264–A3290.